Lappeenranta University of Technology
Faculty of Technology
LUT Energy

MODEL-BASED STUDY OF A CHEMICAL-LOOPING COMBUSTION PROCESS

Examiner: Professor Timo Hyppänen
Instructor: D.Sc. Tero Tynjälä

Lappeenranta 12.08.2009

Petteri Peltola
Orioninkatu 7 A 7
53850 Lappeenranta
+358503657889

ABSTRACT

Lappeenranta University of Technology
Faculty of Technology
Degree Programme in Energy Technology

Petteri Peltola

Model-based study of a chemical-looping combustion process

Master's thesis
2009

68 pages, 22 figures, 8 tables

Examiner: Professor Timo Hyppänen
Instructor: D.Sc. Tero Tynjälä

Keywords: air reactor, chemical-looping combustion, fuel reactor, oxidizer, oxygen carrier, reducer

Chemical-looping combustion (CLC) is a novel combustion technology with inherent separation of the greenhouse gas CO_2. The technique typically employs a dual fluidized bed system where a metal oxide is used as a solid oxygen carrier that transfers the oxygen from combustion air to the fuel. The oxygen carrier is looping between the air reactor, where it is oxidized by the air, and the fuel reactor, where it is reduced by the fuel. Hence, air is not mixed with the fuel, and outgoing CO_2 does not become diluted by the nitrogen, which gives a possibility to collect the CO_2 from the flue gases after the water vapor is condensed. CLC is being proposed as a promising and energy efficient carbon capture technology, since it can achieve both an increase in power station efficiency simultaneously with low energy penalty from the carbon capture.

The outcome of a comprehensive literature study concerning the current status of CLC development is presented in this thesis. Also, a steady state model of the CLC process, based on the conservation equations of mass and energy, was developed. The model was used to determine the process conditions and to calculate the reactor dimensions of a 100 MWth CLC system with bunsenite (NiO) as oxygen carrier and methane (CH_4) as fuel.

This study has been made in *Oxygen Carriers and Their Industrial Applications* research project (2008 – 2011), funded by the *Tekes – Functional Material* program. I would like to acknowledge Tekes and participating companies for funding and all project partners for good and comfortable cooperation.

TIIVISTELMÄ

Lappeenrannan teknillinen yliopisto
Teknillinen tiedekunta
Energiatekniikan koulutusohjelma

Petteri Peltola

Kemikaalikierrollisen polttoprosessin malliperusteinen tarkastelu

Diplomityö
2009

68 sivua, 22 kuvaa, 8 taulukkoa

Tarkastaja: professori Timo Hyppänen
Ohjaaja: TkT Tero Tynjälä

Hakusanat: hapenkantaja, ilmareaktori, kemikaalikierto, polttoainereaktori

Kemikaalikiertoon perustuva polttoprosessi (chemical-looping combustion, CLC) on uudenlainen hiilidioksidin talteenottomenetelmä, missä CO_2:n erottaminen savukaasuista tapahtuu luonnollisena osana itse prosessia. CLC-systeemi muodostuu tavallisesti kahdesta toisiinsa yhteydessä olevasta leijupetikattilasta, joiden välillä kiertää metallioksidipartikkeleita ns. hapenkantajina. Ilmareaktoriin syötettävä polttoilma hapettaa partikkelit, minkä jälkeen ne pelkistyvät polttoainereaktorissa luovuttaen hapen polttoaineeseen. Koska ilma ei sellaisenaan osallistu palamiseen, ei polttoainereaktorin jälkeinen savukaasuseos sisällä typpeä, mikä helpottaa huomattavasti hiilidioksidin talteenottoa. CLC nähdään yhtenä varteenotettavana CO_2:n talteenottoteknologiana, koska sen avulla voidaan parantaa sekä palamisprosessin että talteenoton energiahyötysuhdetta.

Tässä työssä esitetään tärkeimmät tulokset kattavasta kirjallisuusselvityksestä, jossa pyrittiin luomaan laaja-alainen katsaus CLC-tutkimuksen nykytilaan. Lisäksi kehitettiin aine- ja energiataseisiin perustuva stationäärinen CLC-prosessimalli, jonka avulla määritettiin 100 MWth:n CLC-systeemin prosessiolosuhteet ja reaktorigeometria. Hapenkantajana prosessissa toimi bunseniitti (NiO).

Työ on tehty osana *Hapen kuljetusmateriaalit ja niiden teollisuussovellukset* – tutkimusprojektia (2008 – 2011), joka kuuluu *Tekes – toiminnaliset materiaalit* – ohjelmaan. Haluan kiittää Tekesiä sekä ohjelmaan osallistuvia yrityksiä rahoituksesta. Esitän myös kiitokseni hedelmällisestä yhteistyöstä niille tahoille, joiden kanssa sain olla tekemisissä projektin aikana.

ACKNOWLEDGEMENTS

I would like to thank my supervisor, Tero Tynjälä, for his guidance and continuous support for my Master's Thesis. I would also like to thank Professor Timo Hyppänen for the subject of the Thesis and giving me the opportunity to work with this interesting topic. Thanks also to my colleagues here in the laboratory of Modelling of Energy Systems – it have been a pleasure to work with you.

Special thanks to my family members in Kotka. I greatly appreciate the support you have given me in many ways during my studies. Also many thanks to my better half here in Lappeenranta!

TABLE OF CONTENTS

LIST OF SYMBOLS

A	area	m^2
Ar	Archimedes number	-
c_p	specific heat capacity	J/kgK
C_D	drag coefficient	-
d_p	particle diameter	mm
g	gravitational acceleration	m/s^2
h	specific enthalpy	kJ/kg
h_c	heat transfer coefficient	W/m^2K
h_0	correlation constant	-
H	height	m
ΔH_c	heat of combustion	kJ/mol
ΔH_{oxd}	oxidation enthalpy	kJ/mol
ΔH_{red}	reduction enthalpy	kJ/mol
m	mass	kg
M	molar mass	g/mol
n	isentropic coefficient	-
p	pressure	bar
P	power	MW
Δp	pressure drop	kPa
$q_{i,CH4}$	lower heating value of methane	MJ/kg
q_m	mass flow	kg/s
q_V	volumetric flow	m^3/s
R	universal gas constant	J/molK
R_o	oxygen ratio	-
Re	Reynolds number	-
T	temperature	°C, K

u	superficial gas velocity	m/s
u_{mf}	minimum fluidizing velocity	m/s
u_T	particle terminal velocity	m/s
Δu_{th}	difference in superficial gas velocity and particle terminal velocity at threshold point	m/s
v	specific volume	m^3/kg
V	volume	m^3
w	weight fraction	-
x	recirculation ratio	-
X_{oxd}	degree of oxidation	-
X_{red}	degree of reduction	-
ΔX	conversion difference	-

Greek letters

α	correlation constant	-
ε	voidage	-
ϕ_s	particle roundness	-
φ_{fan}	fractional fan power	-
Φ	heat output	MW
η	efficiency	-
λ	air ratio	-
μ	dynamic viscosity	kg/ms
ρ	density	kg/m^3
τ	particle residence time	s

LIST OF FIGURES

Figure 22. Example case: Bed mass in the reactor as a function of the degree of reaction..

LIST OF TABLES

1 INTRODUCTION

1.1 Background

The world climate and the long-term impact of climate change have been under critical discussion during the last decade. Significant studies associated with climate warming have shown that the mean annual temperature at the earth's surface is increasing due to the acts of human. The total temperature increase from 1850 – 1899 to 2001 – 2005 is 0.76 °C and it is assumed to rise further, 1.1 to 6.4 °C during the 21st century (IPCC, 2001).

The main contributor to the global warming is emission of greenhouse gases, e.g. CO_2, SO_X, NO_X and CH_4. It has been established, that CO_2 is the most important anthropogenic greenhouse gas, while it has direct effects to the climate warming process. According to the statistics, the emission of CO_2 resulting from human activity have led to an increase in the atmospheric CO_2 concentration, from a pre-industrial level of 280 ppm to 380 ppm (IPCC, 2001).

Since the beginning of the industrial era, fossil fuels have been a great source of energy for the global economy. In 2001, non-renewable fuels accounted 83 % of the energy supply in OECD countries and 76 % in the rest of the world (IEA, 2003). As energy use has increased, greenhouse gas emissions have spiraled up. Combustion of fossil fuels releases a massive amount of carbon dioxide into the atmosphere among other combustion gases.

It is estimated that power production contributes with one-third of CO_2 released from fossil fuel combustion world-wide (Lyngfelt et al., 2001), and so there is a great interest to develop CO_2-free power production methods. It can be assumed, that alternative energy technologies can scarcely fully replace the existing fossil fuels based power generation. Thus, power production via combustion of fossil fuels with effective CO_2 capture is going to be in a key role what comes to the energy supply in the foreseeable future.

For the moment there are some commercially available industrial-scale processes in order to capture CO_2: (i) pre-combustion is a technique to remove the carbon from fuel before it is burned, based on fuel gasification, (ii) oxy-fuel combustion uses oxygen-enriched gas mixture instead of air and (iii) post-combustion, in which CO_2 is separated from the flue gases using suitable methods. After the separation, CO_2 must be stored economically and environmentally friendly. Several possibilities for such storage have been proposed: storage in used oil and gas fields, in deep goal beds, in deep sea bottom or in aquifers. Existing separation techniques are very energy intensive and if used, they tend to decrease the overall combustion efficiency, which eventually affects the price of produced electricity. This decrease in efficiency alone increases the cost for electricity production with one-fourth. It is estimated, that the cost of CO_2 separation is 63 – 126 €/ton C, which is much compared to the costs for disposal of CO_2, ranging 2.5 – 5 €/ton C (Lyngfelt et al., 2001).

First introduced in the 1980's (Ishida, et al. 1987; Richter & Knoche, 1983), the chemical-looping combustion (CLC) appears to have the potential for delivering the most efficient and economic technology in case of carbon capture and storage (CCS). CLC is based on a metal oxide as an oxygen carrier, which transfers oxygen from combustion air to the fuel, whereupon the direct contact between air and fuel is avoided. In CLC, the separation of CO_2 is inherent and it is dealing with minimum energy losses. Furthermore, CLC can be adapted for the production of hydrogen and as well, with inherent CO_2 capture.

1.2 Thesis objective and structure

The aim of this thesis was to study the physical bases of chemical-looping combustion, in order to gain better understanding of the process and its operation. At first, a comprehensive literature study about the current situation in CLC research was performed. Chapter 2 contains the outcome of this state-of-the-art-study. Some observations from the literature part were used as design criteria in chapter 3, where a steady state CLC process model, based on conservation equations of mass and energy, is presented.

The model was used to determine the process conditions and to calculate the reactor dimensions of a 100 MWth CLC system with bunsenite (NiO) as oxygen carrier and methane (CH_4) as fuel. Results are given and discussed in chapter 4.

2 CHEMICAL-LOOPING COMBUSTION

CLC process was originally suggested to increase thermal efficiency in power generation station, but later on its advantages for effective CO_2 separation were discovered (Ishida et al., 1987; Richter & Knoche, 1983). Although the principles of the process have been known for quarter of a century, the majority of work related to CLC is done within the last decade.

In traditional combustion the fuel is in direct contact with air. Most of the technologies using this combustion method require a large amount of energy to separate and collect CO_2 from the exhaust gas, because CO_2 is diluted by N_2 of the combustion air. The conventional gas-phase combustion reaction, when using air as the oxygen source, is exothermic and can be written

$$C_xH_y + (x + \frac{y}{4})O_2 + 3.76(x + \frac{y}{4}) \rightarrow xCO_2 + \frac{y}{2}H_2O + 3.76(x + \frac{y}{4}) \qquad (2.1)$$

In CLC system, the process shown in Figure 1 is split into two interconnected fluidized bed reactors: an air reactor and a fuel reactor where two consecutive gas-solid reactions forming a chemical loop occur. A solid oxygen carrier (metal oxide) is used to transfer the oxygen from the air to the fuel. The oxygen carrier is looping between the air reactor, where it is oxidized by the air (Eq. 2.2), and the fuel reactor, where it is reduced by the fuel (Eq. 2.3). Hence, the air is not mixed with the fuel, and the CO_2 does not become diluted by the nitrogen. The outgoing gas from the oxidation step will contain N_2 and unreacted O_2, while the gas from the reduction step will be mixture of CO_2 and water vapor. The water vapor can be condensed, and close to pure CO_2 is then obtained with minor losses of energy. Some energy is still needed, however, to compress the CO_2 into a liquid form, suitable for transportation and storing. (Lyngfelt et al., 2001).

Oxidation in the air reactor:

$$\mathrm{Me} + \frac{1}{2}\mathrm{O_2} \rightarrow \mathrm{MeO} \tag{2.2}$$

Reduction in the fuel reactor:

$$(2x + y)\mathrm{MeO} + \mathrm{C_xH_{2y}} \rightarrow (2x + y)\mathrm{Me} + y\mathrm{H_2O} + x\mathrm{CO_2} \tag{2.3}$$

Depending upon the used metal oxide, the reduction reaction is often endothermic ($\Delta H_{\mathrm{red}} > 0$), while the oxidation reaction is highly exothermic ($\Delta H_{\mathrm{oxd}} < 0$). The total amount of released heat ΔH_{c} is the same as for normal combustion.

$$\Delta H_{\mathrm{c}} = \Delta H_{\mathrm{red}} + \Delta H_{\mathrm{oxd}} < 0 \tag{2.4}$$

where ΔH_{c} is the heat of combustion

ΔH_{red} is the heat of reduction

ΔH_{oxd} is the heat of oxidation.

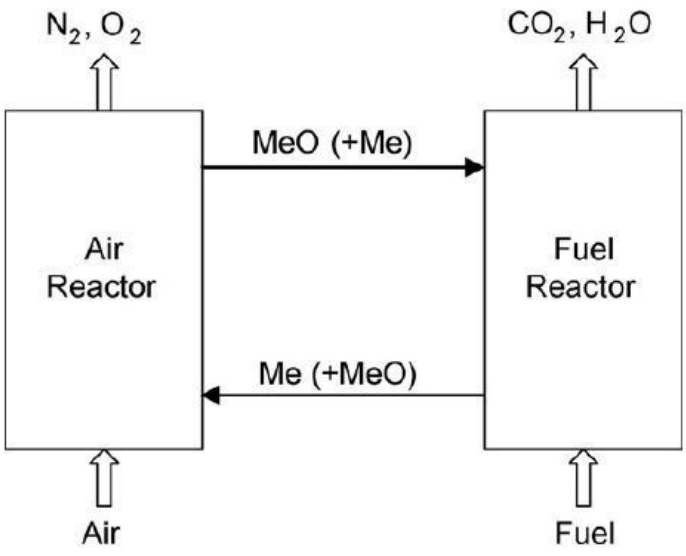

Figure 1. CLC process loop between two interconnected fluidized bed reactors (Lyngfelt et al., 2001).

CLC also minimizes the formation of thermal NO_X, because the combustion environment in the fuel reactor is air-free, and the reaction temperature (< 1200 ºC) in the air reactor is well below the temperature (> 1500 ºC) wherein NO_X particles begin to form.

2.1 Reactor design

Reactor design of a chemical-looping combustor must be contrived carefully. Intimate contact between the oxygen carrier and gas phase species is important in order to obtain high performance in CLC, and given phase contacting is strongly related to the reactor configuration. A suitable reactor system in a combined cycle has to meet the following requirements (Wolf, 2004):

- Enable adequate particle transport between the air reactor and the fuel reactor to guarantee an efficient fuel conversion
- Provide a sufficient reaction time for the reactions
- Prevent gas exchange between the two reactors
- Reach a sufficiently high temperature in the outlet of the reactor
- Withstand the required pressure.

Lyngfelt et al. (2001) proposed a circulating system composed of two connected fluidized beds: high-velocity riser as an oxygen reactor and low-velocity bubbling bed as a fuel reactor (Fig. 2). The solid particles leaving the riser are recovered by a cyclone and sent to the fuel reactor. The fuel reactor is located at a relatively high level, thus the reduced particles are returned to the air reactor by means of gravity.

In the configuration of interconnected fluidized beds like this, there is a possibility of gas leakage which must be minimized. Fuel gas leakage from the fuel reactor to the riser results carbon dioxide release into the atmosphere, reducing the efficiency of the carbon capture process. Leakage of air from the riser to the fuel reactor dilutes the combustion gas with N_2, which adds extra costs to the CO_2 separation. Leakage between the reactors can be reduced with two gas locks, one placed between the cyclone and the fuel reactor and the other between the fuel reactor and the riser. (Lyngfelt et al., 2001).

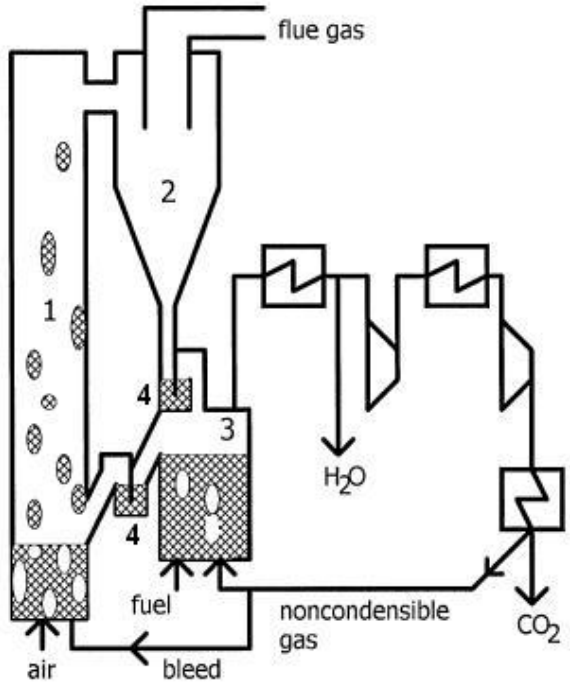

Figure 2. Chemical-looping combustion reactor layout. 1) Air reactor, 2) cyclone, 3) fuel reactor, 4) particle locks (Lyngfelt et al., 2001).

Flue gas from the fuel reactor contains mainly CO_2 and H_2O, but there can also be minor amount of unreacted fuel, such as methane. After condensation of the water, the remaining gas is compressed and cooled to yield liquid CO_2, while non-condensable fuel gas is recycled back to the fuel reactor. Some part of this flow is bled to the air reactor, in order to avoid accumulation of non-combustible gases, like N_2. (Lyngfelt et al., 2001).

The volumetric gas flow in the riser is approximately ten times larger than that of the gaseous fuel in the fuel reactor. High gas velocity is chosen in the air reactor in order to keep a moderate size of the reactors.

2.2 Oxygen carriers

Oxygen carriers play an important role what comes to the performance of the CLC process. For example, the amount of the bed material in both reactors and the circulation rates of solids between these reactors are mainly depended on the characteristics of the chosen oxygen carrier. The metal oxide used as an oxygen carrier should have the following features (Lyngfelt et al., 2001; Adánez et al., 2004; Hossain & Lasa, 2008):

- Sufficient rates of oxidation and reduction
- Adequate durability in successive cycle reactions under high temperature
- Enough mechanical strength to limit particle breakage, attrition and wear
- Resistance against carbon deposition
- Resistance to agglomeration
- Environmentally safe
- Technically and economically feasible.

Ideally thinking, the number of reaction cycles of the oxygen carrier would be infinite. Regardless, the carrier particles must be periodically replaced as a consequence of mechanical wear and reactivity loss during the cycles. In general, suitable metal oxides

are combined with an inert which acts as a porous support providing a higher surface area for reaction, better mechanical strength and attrition resistance, and, in addition, as an ion conductor enhancing the ion permeability in the solid (Adánez et al., 2004). In Figure 3 can be seen the shape and surface structure of Mn-based oxygen carrier supported with zirconia.

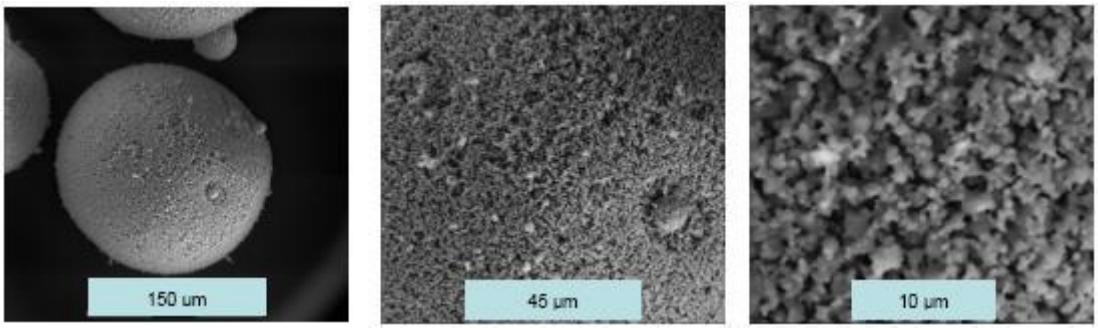

Figure 3. Oxygen carrier composed of 40 % Mn_3O_4 on 60 % partially stabilized zirconia Mg-ZrO_2 (Mattisson et al., 2006a).

In the literature, a number of metals and their corresponding oxides have been referred as possible carriers: copper, nickel, cadmium, manganese, cobalt and iron. As well, many inert materials have been suggested, e.g. Al_2O_3, SiO2, TiO_2, ZrO_2 and sepiolite. The majority of the previous and current research studies consider three promising carrier candidates – Fe, Cu and Ni – because of the favorable thermodynamics, plentiful availability and low cost of both iron- and copper-based oxygen carriers, and on the other hand, the superior reactivity of nickel-based materials (Hossain & Lasa, 2008). Table 1 shows the schematic reactions of Fe, Cu, and Ni used in CLC.

One of the main areas in current CLC research is the oxygen carrier development. To this day, great amount of work is done in order to find the best possible metal oxide/inert combination. The work is challenging due to the intricate premises; reactivity performance is very dependent upon oxygen carrier system, particle preparation method, particle size, fuel gas and reactor type among many other variables.

Table 1. Reactions of the metal oxides used in CLC and heat of the combustion at standard conditions (298.15 K, 0,1 MPa) (Adánez et al., 2006).

MeO/Me		ΔH_c^0 (kJ/mol)
CuO/Cu		
	$CH_4 + 4CuO \rightarrow 4Cu + CO_2 + 2H_2O$	-178.0
	$H_2 + CuO \rightarrow Cu + H_2O$	-85.8
	$CO + CuO \rightarrow Cu + CO$	-126.9
	$O_2 + 2Cu \rightarrow 2CuO$	-312.1
NiO/Ni		
	$CH_4 + 4NiO \rightarrow 4Ni + CO_2 + 2H_2O$	156.5
	$H_2 + NiO \rightarrow Ni + H_2O$	-2.1
	$CO + NiO \rightarrow Ni + CO_2$	-43.3
	$O_2 + 2Ni \rightarrow 2NiO$	-479.4
Fe_2O_3/Fe_3O_4		
	$CH_4 + 12Fe_2O_3 \rightarrow 8Fe_3O_4 + CO_2 + 2H_2O$	141.6
	$H_2 + 3Fe_2O_3 \rightarrow 2Fe_3O_4 + H_2O$	-5.8
	$CO + 3Fe_2O_3 \rightarrow 2Fe_3O_4 + CO_2$	-47.0
	$O_2 + 4Fe_3O_4 \rightarrow 6Fe_2O_3$	-471.9

2.2.1 Reactivity and oxygen ratio

The reactivity of the oxygen carriers in both oxidation and reduction cycles is an important factor to be considered in the design of a CLC process, because it is related to the solids inventory in the system. The bed mass in the real system is inversely proportional to the reaction rate of the oxygen carriers, so the higher reaction rate means the smaller bed mass needed, and as well, smaller reactor sizes and less production costs. The carrier must be reactive enough to fully convert the fuel gas in the fuel reactor, and to be reoxidized in the air reactor.

Some general conclusions about the reactivity can be made from the literature (Mattisson et al., 2006b):

- Reactivity generally increases as a function of reaction temperature, although high reactivity has also been seen at rather low temperatures in some cases

- The reduction reactivity is faster with syngas (H_2, CO) than CH_4 as fuel

- Nickel oxides and copper oxides are considered as the most reactive carrier materials so far

- Nickel oxides can not fully convert the fuel gases to CO_2 and H_2O, and reduced Ni catalyzes carbon formation and steam reforming.

Another important characteristic of the metal oxide is its oxygen transport capacity, also called the oxygen ratio, R_o, and defined as

$$R_o = \frac{M_{ox} - M_{red}}{M_{ox}} \tag{2.5}$$

where M_{ox} is the molar mass of fully oxidized oxygen carrier

M_{red} is the molar mass of fully reduced oxygen carrier

As seen in Figure 4, the higher values of oxygen transport capacities correspond to NiO and CuO, and it is lower for Fe_2O_3 in its transformation to Fe_3O_4. In spite of the different oxidation states of iron compounds, only the transformation from hematite (Fe_2O_3) to magnetite (Fe_3O_4) may be suitable for CLC systems. The hematite reaction rates to metallic iron are slow, and further reduction to wüstite (FeO) would led to a high decrease in the purity of CO_2 obtained in the fuel reactor due to the increase of CO and H_2 concentrations in the equilibrium. The transport capacity of the oxygen carriers obviously decrease with the addition of the inert. (Adánez et al., 2006).

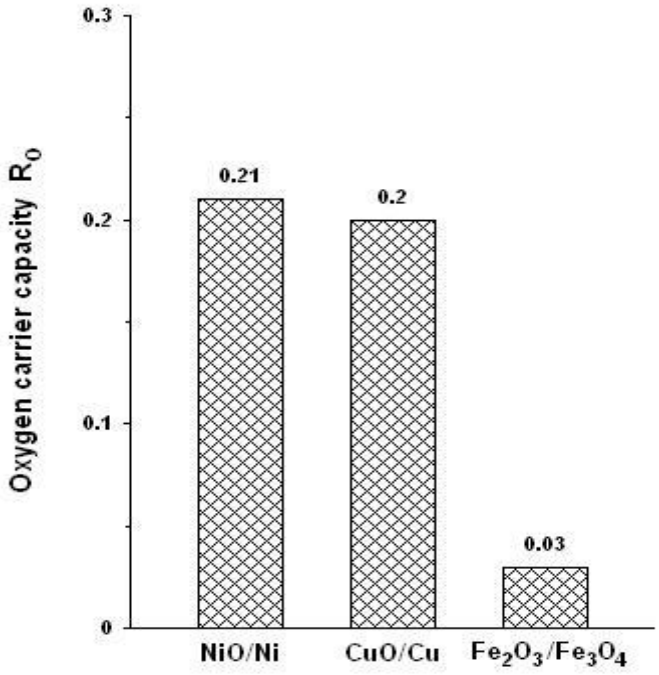

Figure 4. Oxygen ratios of Ni-, Cu- and Fe-oxides.

Reactivity experiments simulating CLC and using natural ores or pure metal oxides as the oxygen carriers, without the presence of inert, have shown rapid degeneration or low reaction rates of these materials. To achieve higher reactivity and get more stabilized oxygen carriers, these could be prepared synthetically and mixed with an inert material. It is believed, that the porosity of the particles is increased with the addition of inert, and due to that, the oxidation and reduction rates of the carrier will be higher. Inert also helps to maintain the structure and increases the ionic conductivity of the particle, but on the other hand, it decreases the ratio of free oxygen. (Johansson, 2007).

2.2.2 Melting point and mechanical strength

The temperature, in which the CLC process is assumed to operate, is between 600 °C and 1200 °C (Hossain & Lasa, 2008). This will create some constraints on the oxygen carrier selection. The melting point of the oxygen carrier should be high enough to withstand the CLC reaction temperature and to avoid agglomeration of circulating particles. Melting points of some potentially suitable metals and inerts are listed in Table

2. As seen, Cu has a relatively low melting point, and therefore it cannot be used above 900 °C.

Table 2. Physical properties of solids (García-Labiano et al., 2004).

	Solid density, ρ_s (kgm^{-3})	Melting point (°C)
Active material		
Cu	8920	1085
CuO	6400	1124 *
Ni	8900	1453
NiO	6670	1955
Fe	6980	1536
FeO	5700	1377
Fe_2O_3	5240	1462 *
Fe_3O_4	5180	1597
Inert		
Al_2O_3	3965	2017
SiO_2	2260	1723
TiO_2	4260	1857
ZrO_2	5600	2677
MgO	3580	2832

* Normal decomposition point

Adánez et al. (2004) studied the mechanical strength of different oxygen carriers. Measured values are shown in Table 3. As a conclusion, the crushing strength seems to be strongly dependent on the type of active metal oxide and its concentration, the inert used as a binder and the sintering temperature. In general, a higher sintering temperature increases the crushing strength, but some carriers cannot withdraw high temperatures due to decomposition and melting of the involved compounds. Fe-based oxygen carriers prepared with Al_2O_3, TiO_2, and ZrO_2 and sintered above 1100 °C showed high crushing strength values. Cu-based carriers did not show measurable values, excepting

when using SiO_2 or TiO_2 as inerts. Combinations of Ni and TiO_2 or Ni and SiO_2 showed satisfying values.

Table 3. Crushing strength (N/mm) of the studied metal oxide/inert compounds (Adánez et al., 2004).

		Metal-based oxygen carriers											
		Fe				Ni				Cu			
Inert	T_{sint} (°C) MeO (%)	950	1100	1200	1300	950	1100	1200	1300	950	1100	1200	1300
Al_2O_3	80	0	13	105	61	0	0	0	0	3	5		
	60	0	12	17	57	0	0	0	0	0	0		
	40	0	12	22	65	0	2	3	4	0	0		
SiO_2	80	12	60			0	1	11*	25*	22			
	60	15	85			6	16	32	45	20			
	40	10	52			22	39	35		17			
TiO_2	80	12	71	111	17	1	16	42	50	66			
	60	21	45	36	11	4	17	32	48	59			
	40	40	94	81	30	14	23	33	65	43			
ZrO_2	80	3	25	33	76	0	2	1	3	6			
	60	12	20	29	54	0	0	3	5	2			
	40	13	19	19	56	0	3	13*	11*	1			
Sepio-lite	80	9	48			0	1	4	120	4			
	60	7	20			1	6	14*		0			
	40	1	14			0	3	53		0			

Melt or decompose

Soft

* Broken after 5 cycles

2.2.3 Additional factors affecting the oxygen carrier properties

Effect of the sintering temperature. When preparing the oxygen carrier material, sintering in high temperature is used to create hard and enduring particles, and in some

cases, to advance creation of a new inert material, like $NiAl_2O_4$. The higher crushing strength of the oxygen carrier is supposed to extend the lifetime of the particles in a fluidized bed reactor, and therefore, the aim is to create particles that are not too soft and do not have the tendency to fragmentize. One way to do this is to adjust the sintering temperature, which results in an increase of the apparent density and the crushing strength. Regardless, sintering decreases the particle reactivity due to the diminished porosity. Figure 5 outlines the correlation between crushing strength and sintering temperature for Mn-based oxygen carriers on stabilized and un-stabilized zirconia. (Johansson, 2007).

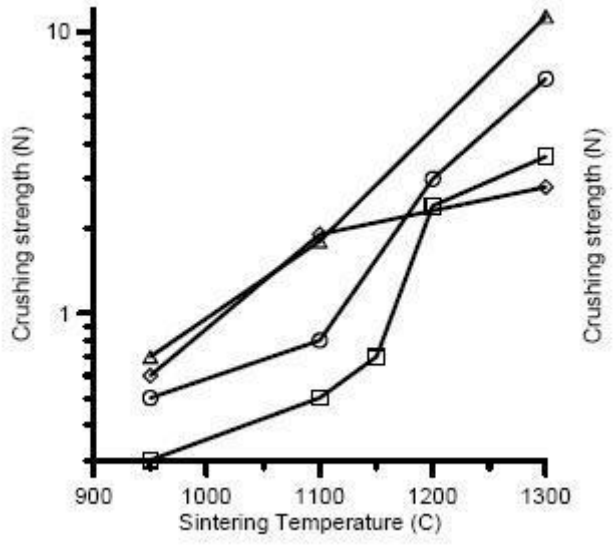

Figure 5. Crushing strength for some Mn-based oxygen carriers as a function of sintering temperature. M4Z (◊), M4CaZ (○), M4MgZ (□), M4CeZ (Δ) (Johansson, 2007).

Effect of the particle size. The size of the oxygen carrier particles has effects on the oxidation and reduction rates, as well on the external mass and heat transfer processes. An increase in the particle size leads to a decrease in the reaction rates, but the heat transfer intensifies due to particle's greater thermal capacity, and that makes it hard to come to a decision on the optimal particle size. The studies have concentrated on the particles ranging from 0.1 to 2.0 mm. Yet, no applicable correlation between particle's size and its performance in the system has been established.

Effect of the particle porosity. The optimum particle porosity is basically a compromise between the reactivity, avoiding diffusion resistances inside the particle, and the

crushing strength with low attrition rates. An increase in the particle porosity produces an important increase in the reaction rate because of the lower gas diffusion resistance in the pore system, but at the same time the crushing strength decreases somewhat. (García-Labiano et al., 2004).

2.3 Design procedure for a CLC system

Kronberger et al. (2005) introduced an exhaustive design procedure for a CLC process. It considers reaction kinetics, hydrodynamics, mass and heat balances, and reactor geometry, which are determined by the design input data, as desired power output, chosen oxygen carrier, and fuel type. Figure 6 shows, how different design specifications and operational features, are linked together.

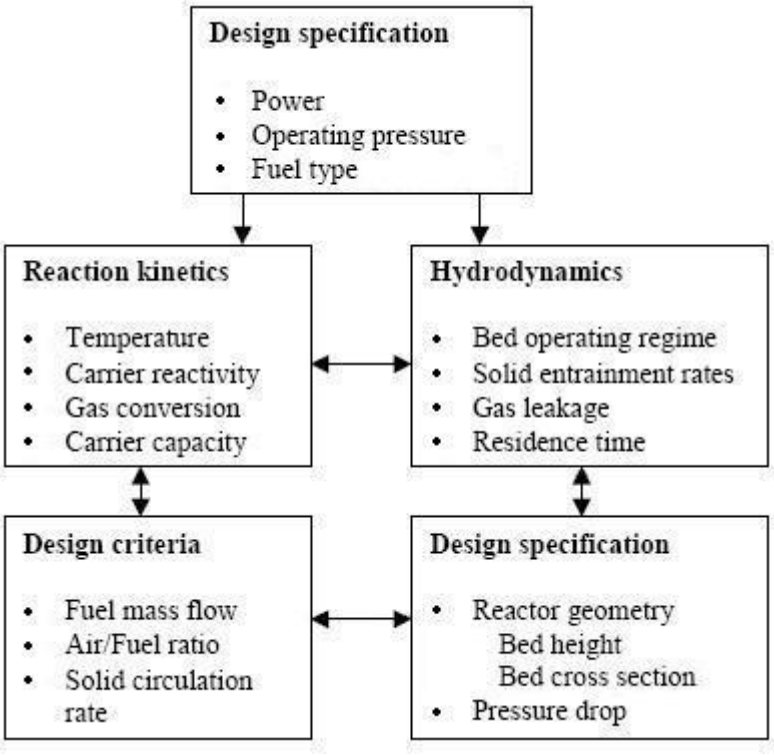

Figure 6. Design procedure for a CLC system (Kronberger et al., 2005).

2.3.1 Mass and heat balances

The fuel and air mass flows, thus the air-to-fuel ratio, are determined by the desired power output. The most crucial input data is the type of the oxygen carrier. It determines both the amount of bed material in the two reactors, which must be adequate to maintain sufficient conversion of reacting gas, and the circulation rate of solids between the reactors, which must be high enough to transfer the needed amount of oxygen for the fuel combustion. These two parameters are mainly dependent on the characteristics of the chosen carrier, as solid reactivity, type of the metal oxide and, and weight content. A high reaction rate means a smaller bed mass needed, while the solids circulation rate in the system is a function of the difference in conversion, ΔX, between particles in the riser and the fuel reactor. The conversion, or gas yield, of the fuel is also a crucial parameter. The unconverted gas from the fuel reactor must be either re-circulated back or burned off by adding oxygen downstream of the fuel reactor, which will increase costs and complexity of the system (Johansson, 2007). Figure 7 shows the design data related to the oxygen carrier properties.

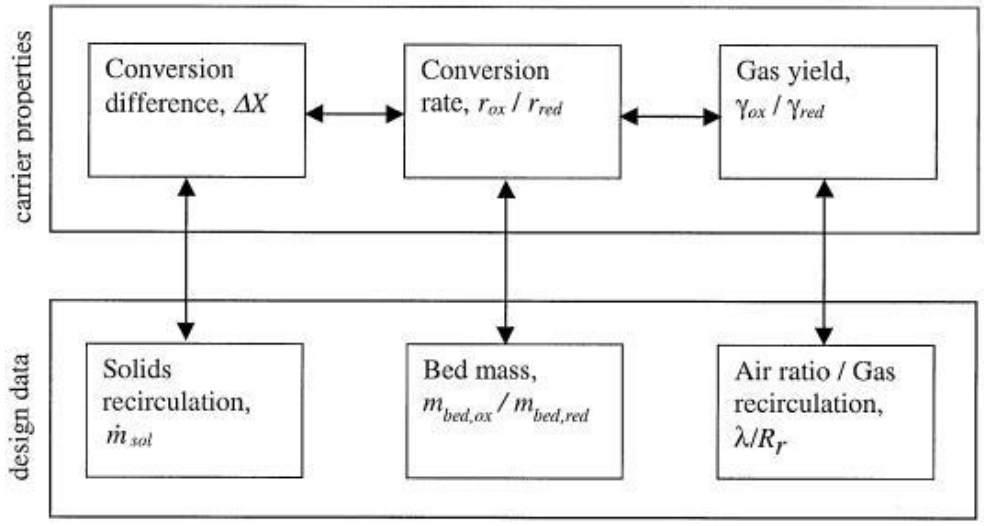

Figure 7. The basic relations between design input data and carrier reactivity (Lyngfelt et al., 2001).

2.3.2 Fluidization velocities

The CLC system is composed of two interconnected fluidized beds: an air reactor and a fuel reactor. A high-velocity riser acts as an air reactor, and its operating conditions predominantly determine the hydrodynamics of the CFB system. Velocities congruent with typical CFB risers are desired. The assumed gas velocity is 4 – 10 times the terminal velocity, which will induce sufficient solids entrainment for the required circulation rates of particles. The widened bottom section of the riser causes a higher mean particle residence time in the oxidation zone. Appropriate velocities in this zone are 1.2 – 3 times the terminal velocity.

Most oxygen carrier types demand a relatively high particle residence time for the fuel oxidation, so the stationary bed of the fuel reactor is operating in the bubbling fluidized bed regime. Low gas velocities below 0.7 times the terminal settling velocity and above 2 times the minimum fluidization velocity, depending on the thermal power and oxygen carrier properties, are advisable design parameters. (Kronberger et al., 2005).

2.3.3 Temperature and pressure

According to Lyngfelt et al. (2001), there are few important aspects to be considered in the choice of process temperature. A higher temperature, in general, enhances the reaction rates and reduces the needed amount of bed material. An extremely high temperature may cause technical problems, such as sintering of bed material. In the case of a power generation, a higher temperature is essential for gaining a high thermal efficiency. Because of the endothermic reactions in the fuel reactor, there can be a temperature drop, which must be minimized by ensuring a sufficient recirculation mass flow.

The CLC system will be included in a combined gas turbine or steam power cycle, and it should be designed for use under pressurized conditions in order to achieve a high overall efficiency of electricity production. As with the process temperature, a higher pressure is expected to give higher reaction rates, and furthermore, a greater cross-

sectional mass flow of gas is achievable due to the higher density of the gas. (Lyngfelt et al., 2001).

The pressure drop of both fluidized beds is determined by the bed height, which itself is governed by the required particle residence time. The pressure drop in the air reactor is similar to that of CFB combustors, but higher in the fuel reactor because of the lower conversion rates of reduction (Lyngfelt et al., 2001). Overall, the bed mass in each section determines the pressure conditions of the system, i.e. the pressure loop. That must be carefully considered as, for example, too large of a pressure difference between the reactors can cause problems with the particle locks (Kronberger et al., 2005).

2.3.4 Gas leakage between the reactors

Gas leakage between the reactors is difficult to avoid completely. The leakage can be reduced by loop seals, and in addition, the pressure in the two reactors should be approximately equal. However, if gas can leak from the reducer to the oxidizer, non-processed carbon dioxide will be released into the atmosphere, leading to a reduced efficiency of CO_2 capture. A leakage of gas in the opposite direction will increase the costs of CO_2 compression, because the exhaust gas is then diluted with nitrogen from the combustion air. (Kronberger et al., 2005).

2.3.5 Emissions of gas, liquid and solids

CLC system is dealing with relatively low emission rates. The combustion air introduced in the air reactor does not give any harmful emissions, because the temperature is too low for the formation of thermal NO_X. The leakage of combustible gases from the fuel reactor to the riser causes minor release of oxidized CO_2 and water into the atmosphere.

The condensed water from the reducer gas can contain some amounts of combustible gases, but the formation of organic compounds is not expected. However, the condensed water can be treated in a sewage plant, if necessary.

The oxygen carrier material, or part of it, is supposed to be exchanged during the process due to the reactivity loss of the particles. Removed material has to be handled outside the reactors, considering health and environmental aspects of it. (Lyngfelt et al., 2001).

2.4 CLC-combined power generation and thermal efficiencies

Several studies related to CLC process performance have proposed relatively high net thermal efficiencies in comparison to processes with conventional combustion methods. For example, Wolf et al. (2001) reported a thermal efficiency as high as 52 – 53 % in combined cycle CLC plant operating at 13 bars and 1200 ºC in the air reactor. Naqvi et al. (2007) presented the net plant efficiency of 52.2 % in the cycle (Fig. 8), where CLC reactors replace combustion chamber of the gas turbine, including CO_2 compression to 200 bars. The efficiency would be something lower in an atmospheric CLC operating in a steam cycle. Still, the results are promising, since they represent somewhat 5 percentage points efficient processes than state-of-the-art technologies for CO_2 capture.

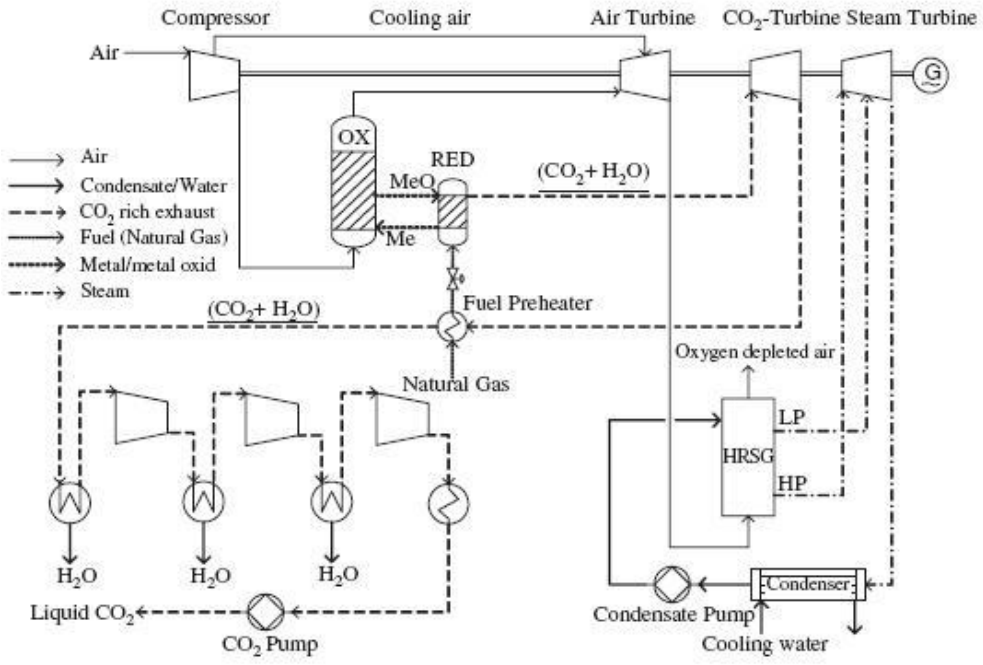

Figure 8. Schematics of the proposed CLC-combined cycle with CO_2 capture (Naqvi et al., 2007).

Successful commercialization of power generation processes with the integration of CLC depends on the development of both specific process configurations and suitable reactor design. Hossain & Lasa (2008) listed important issues that have to be concentrated on:

- The plant configuration
- The possibility of integration with existing power plants
- The operating parameters
- The energy efficiencies
- The economic analysis

Several CLC prototype units have been introduced in the literature. Johansson et al. (2006) presented results from a 300 W laboratory-sized chemical-looping combustor. The system was operated with nickel-based oxygen carriers, and the tests showed a high conversion of the natural gas to carbon dioxide, ranged from 97 to 99.5 %. No methane was detected out from the fuel reactor, and the fraction of CO was between 0.5 and 3 %. Berquerand & Lyngfelt (2008) operated with a 10 kW chemical-looping combustor for solid fuels. South African coal was used as fuel, and ilmenite, a natural iron oxide as oxygen carrier. The tests were conducted at temperatures above 850 °C and for the total test duration of 22 h. The actual CO_2 capture ranged between 82.5 – 96 % while the gas conversion was in the range of 78 – 81 %. Ryu et al. (2004) tested two different types of oxygen carriers with a 50 kW prototype unit. A Ni-based carrier was looping during 3.5 h, and a Co-based carrier during 22 h. The CO_2 concentration of dry flue gases was 98 % for the nickel oxide and 97 % for the cobalt oxide.

2.5 Fuels

Most of the work that has been carried out on CLC in the last decade has focused on natural gas as fuel. Regardless, it would be highly advantageous if the CLC process could be adapted for coal combustion, as coal is much more bountiful and less expensive fossil fuel than natural gas.

2.5.1 Combustion of methane

Common gaseous fuels such as natural gas and refinery gas contain high fraction of methane. The reduction reaction between methane and the oxygen carrier is

$$CH_4 + 4MeO \rightarrow CO_2 + 2H_2O + 4Me \tag{2.6}$$

Depending upon the used metal oxide, the reduction reaction is often endothermic ($\Delta H_{red} > 0$). Although the investigations have shown that the reduction reactivity is faster with syngas (H_2, CO) than methane as fuel, it is a suitable fuel for a first application of the process. (Mattisson et al., 2006b).

In CLC, it is important to be able to convert a high fraction of the incoming fuel to CO_2 and H_2O. Jerndal et al. (2006) studied the degree of methane conversion to carbon dioxide and water with different types of oxygen carriers. To gauge the degree of fuel conversion, the gas yield was defined as the fraction of the fuel which is oxidized to CO_2, and is given by equation

$$\gamma_{CH4} = \frac{p_{CO2}}{(p_{CH4} + p_{CO2} + p_{CO})} \tag{2.7}$$

Here, p_i is the partial pressure of gaseous species in the product gas. Table 4 shows the measured methane yields with different oxygen carriers, and as it can be seen, complete fuel conversion was achieved with carriers based on Cu, Fe and Mn.

Table 4. Measured methane yields at atmospheric pressure (Jerndal et al., 2006).

	γ_{CH4}	
	800 °C	1000 °C
NiO/Ni	0.9949	0.9883
CuO/Cu	1.0000	1.0000
Fe_2O_3/Fe_3O_4	1.0000	1.0000
CdO/Cd	0.9880	0.9827
Mn_2O_3/Mn_3O_4	1.0000	1.0000
CoO/Co	0.9691	0.9299
ZnO/Zn	0.0022	0.0124
$SrSO_4$/SrS	0.9875	0.9738

2.5.2 Combustion of solid fuels

There are basically two ways to perform the CLC with solid fuels. The first route is to use syngas from coal gasification. This gas, consisting mainly of CO and H_2, can be burned in CLC. The gasification needs to be carried out with O_2 in order to obtain undiluted syngas, and thus an energy intensive air separation unit would be needed. The gasification reaction is slow compared to the reaction between the gasified components and the metal oxide particles, and due to that, gasification is the time limiting step of the process (Leion et al., 2008). In comparison to natural gas as fuel, the oxygen carriers are generally more reactive towards both CO and H_2 or the mixture of these (syngas) (Johansson, 2007). The main gasification reactions are:

$$C + H_2O \rightarrow CO + H_2 \quad (2.8)$$

$$CO + H_2O \rightarrow CO_2 + H_2 \quad (2.9)$$

$$C + CO_2 \rightarrow 2CO \quad (2.10)$$

Another option is to introduce the solid fuel directly into the fuel reactor, where the gasification of the coal and subsequent reactions with the metal oxide particles will take place simultaneously. However, the solid-solid reaction between the coal and the metal oxide can be problematic, because it is not very likely to occur at any reasonable rate. As well, a shorter lifetime of the oxygen carriers can be assumed due to the greater attrition rates, when used with solid fuels. Compared to CLC with gaseous fuels, the use of solid fuels will require more advanced reactor design. (Johansson, 2007).

2.5.3 Effects of sulfur species in fuel

Fuels that are considered as potential for CLC can contain some species of sulfur, such as COS, H_2S, mercaptans, and thio-aromatics. These sulfur compounds in natural gas, refinery gas or syngas may react with both the oxygen and the carrier particles in the oxidizer. Oxidation to SO_2 or SO_3, and forming of sulfites or sulfates must be perceived. The formation of solid sulfur compounds is dependent on sulfur species concentrations as well as process conditions. For instance, the oxidation of H_2S is increased at higher temperatures and lower pressures. (Hossain & Lasa, 2007; Jerndal et al., 2006).

Studies show, that Fe-, Cu-, and Mn-based oxygen carriers can convert H_2S fully to SO_2 in the temperature range of 600 – 1200 °C. The degree of conversion is somewhat lower with Ni-based carriers at similar process conditions. Noticing the thermodynamic aspect, the oxygen carriers may be deactivated via the formation of metal sulfides. For example, iron sulfides or sulfates are not allowable in CLC. Therefore, it is highly advantageous to desulfurize the fuel before introduced into the fuel reactor. (Hossain & Lasa, 2007).

2.6 Carbon formation

Under certain conditions carbon deposition is a possible side reaction in CLC. The formation of carbon on the particles will occur most likely through the following reaction mechanisms:

$$CH_4 \rightarrow C + 2H_2 \tag{2.11}$$

$$2CO \rightarrow C + CO_2 \tag{2.12}$$

Equation (2.11) represents the methane pyrolysis, which is dominating at higher temperatures. Equation (2.12) is the Boudouard reaction, and it occurs at lower temperatures. In these reactions the metal acts as a catalyst, instead of a reactant. These reactions are considered undesirable and can be prevented by adjusting the process parameters, such as reaction temperature, pressure, and the mass flow of oxygen into the fuel reactor. Less carbon is formed at higher pressures in the methane pyrolysis and vice versa in the Boudouard reaction. When using CO as fuel, the Boudouard reaction is the only way of carbon formation. Basically, the formation is favored at high pressures, low temperatures and small amounts of added oxygen. If the reaction temperature is above 950 °C and the degree of fuel conversion is adequate, carbon formation should not be a major problem. (Hossain & Lasa, 2008; Jerndal et al., 2006).

Formed carbon can be carried back to the oxidizer causing formation of CO_2, and that has a negative effect on the CO_2 separation efficiency. Therefore, it is important to properly understand the formation mechanisms, and in addition, to investigate the best possible ways to completely avoid or at least minimize the inconvenient formation of carbon.

2.7 Hydrogen production with inherent CO_2 capture

Fossil fuels can be used as a source for hydrogen production. With conventional and commercial processes, the H_2 production results in notable CO_2 emissions into the at-

mosphere. Therefore, CO_2 capture should be possible in large scale industrial facilities of H_2 production.

One future application of chemical-looping technology is a production of hydrogen with inherent CO_2 capture. Two different processes have been proposed:

i) Chemical-looping reforming, and

ii) Steam reforming using chemical-looping combustion.

2.7.1 Chemical-looping reforming

Complete combustion of natural gas requires 2 moles of O_2 per mol CH_4:

$$CH_4 + 2O_2 \rightarrow CO_2 + H_2O \tag{2.13}$$

Partial oxidation of the same fuel requires only a half a mole of O_2 per mol CH_4:

$$CH_4 + ½O_2 \rightarrow CO + 2H_2 \tag{2.14}$$

Chemical-looping reforming of natural gas is similar to CLC, but the amount of air to the air reactor is decreased. At first, the fuel is fully oxidized. Soon, a large part of the oxygen carriers will become reduced due to the lack of free oxygen in the riser, which will eventually lead to partial oxidation of the fuel resulting undiluted stream of H_2, CO, H_2O and CO_2. The definitive composition of this mixture depends on the air ratio. Depending on the purity of required H_2 and the pressure, the CO_2 can be separated by either absorption or adsorption. The same range of oxygen carriers is available for chemical-looping reformation as for chemical-looping combustion, but Ni/NiO as a highly active reformer catalyst seem to be interesting option than the others. Schematic description of the process can be seen in Figure (9). (Johansson, 2007; Rydén, 2008).

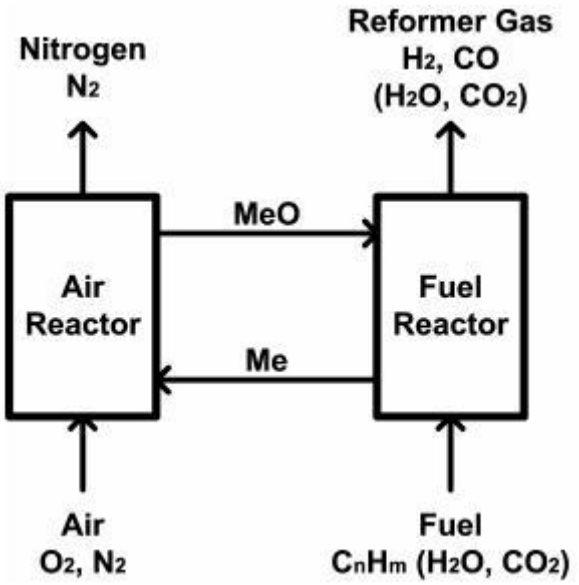

Figure 9. Chemical-looping reforming (Mattisson et al., 2006b).

2.7.2 Steam reforming using chemical-looping combustion

Conventional steam reforming is a process, which is used to convert hydrocarbon fuel to synthesis gas (syngas), consisting mainly of H_2 and CO. Steam reforming of methane, the main component of natural gas, is described by the following reaction:

$$CH_4 + H_2O \rightarrow CO + 3H_2 \tag{2.15}$$

In most present facilities, steam reforming takes place in tubes located inside the furnace. Reformer reactions are highly endothermic, and the required heat is provided by direct firing of a fuel in the furnace. Steam reforming using CLC is slightly different: the reformer tubes are, as well, placed inside the fuel reactor of a CLC unit, but they are not heated by direct firing but rather by the reacting oxygen carrier particles. Steam reforming is followed by water-gas shift, which is an exothermic reaction between CO and H_2O:

$$CO + H_2O \rightarrow CO_2 + H_2 \tag{2.16}$$

After water-gas shift and condensation, high purity H_2 is obtained by pressure swing absorption (PSA). PSA offgas, containing H_2, CO_2, CH_4, and CO, is then led back to the fuel reactor. The proposed design of this process can be seen in Figure 10. (Johansson, 2007; Rydén & Lyngfelt, 2006).

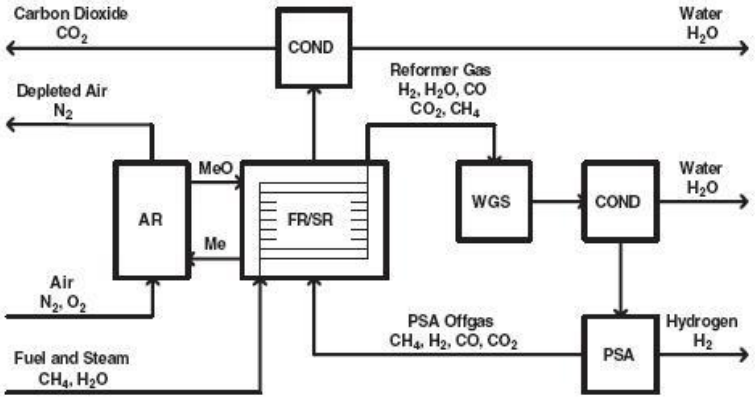

Figure 10. Steam reforming using chemical-looping combustion (Mattisson et al., 2006).

3 PROCESS MODEL

3.1 Design criteria

A full optimization of a CLC system is premature at this state of knowledge. Most of the design data were chosen according to previous experience from conventional CFB boilers. Some of the correlations used in this study will be specified more precisely in the future, when more experimental data will be availabe. A schematic diagram of the simulated system is shown in Figure 11.

- The design criteria were chosen for a boiler that could be used for heat production, for district heating, or for industrial process heat.

- Reactors are simulated as 0-dimensional well-stirred fluidized bed reactors.

- Although pressurized CLC system can achieve higher cycle efficiency, the CLC unit in this study is to be operated at atmospheric pressure.

- Natural gas as fuel is considered to be suitable for the process, although any other gaseous fuel like synthesis gas from goal gasification could be used as well.

- Air reactor's cross-sectional area gives a similar gas velocity as in a CFB combustor.

- Fuel reactor can be considered as a bubbling fluidized bed reactor or as a CFB reactor, depending on the chosen approach.

- The process heat is taken from the air reactor, while the fuel reactor is not cooled. The maximum amount of heat taken from the air reactor is determined by the desired process temperatures.

- The most crucial design input data is the oxygen carrier type. In this study, nickel oxide is used as carrier material and titanium dioxide as supporting inert material.

- The make-up flow of oxygen carrier due to mechanical wear and natural decay of activity during many reduction-oxidation cycles is not considered in this work.

- The pressure drop of both fluidized beds is governed by the bed mass, which it-self follows from the conversion rate and required particle residence time in the reactor.

- Matlab® is used as a modeling platform.

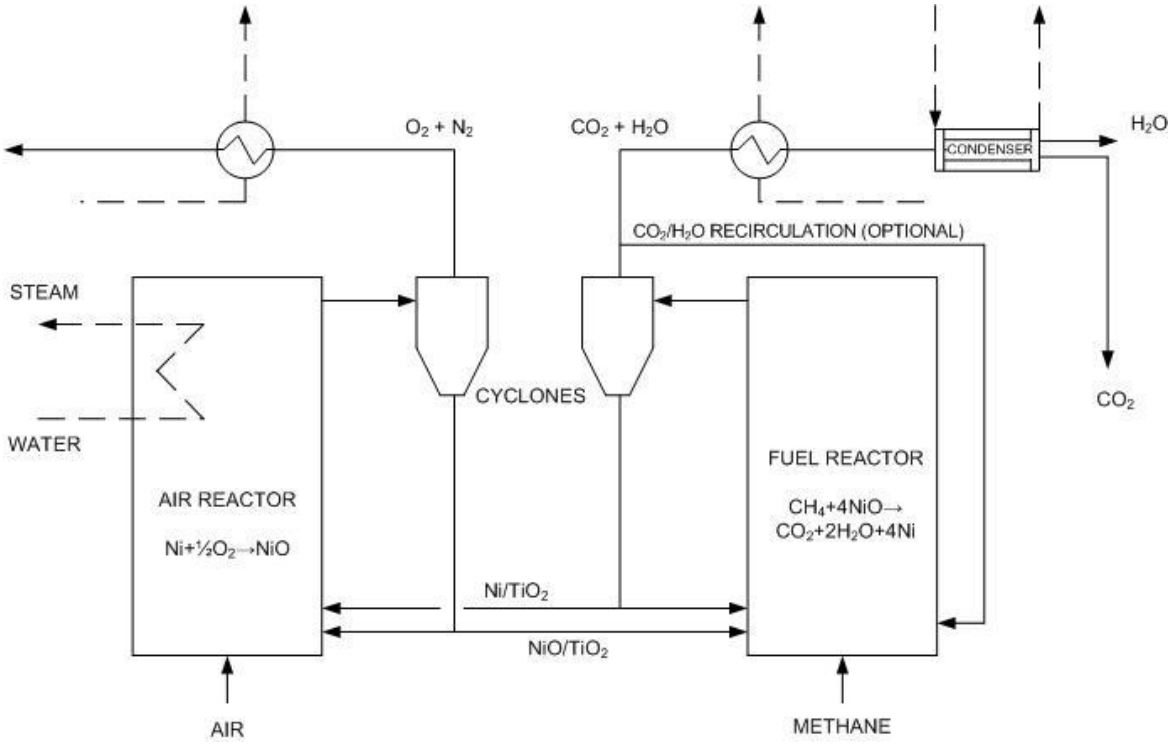

Figure 11. A schematic diagram of the simulated CLC system.

3.2 Model structure and theory

The model is based on the steady state mass and energy balance equations that give reactor temperatures and mass flows of different solids and gases. Appropriate fluidizing velocities in the reactors are determined after the calculation of minimum fluidizing velocity and particle terminal velocity, which both are depended on the oxygen carrier properties.

Solid density profile in the reactor is a function of the fluidizing velocity. Higher gas velocity increases the solids entrainment rate in the freeboard, and thus the heat transfer from the reactor becomes more effective. Overall, exhaustive reactor design is a sum of different aspects and factors that need to be considered carefully. The complete model structure is shown in Figure 12.

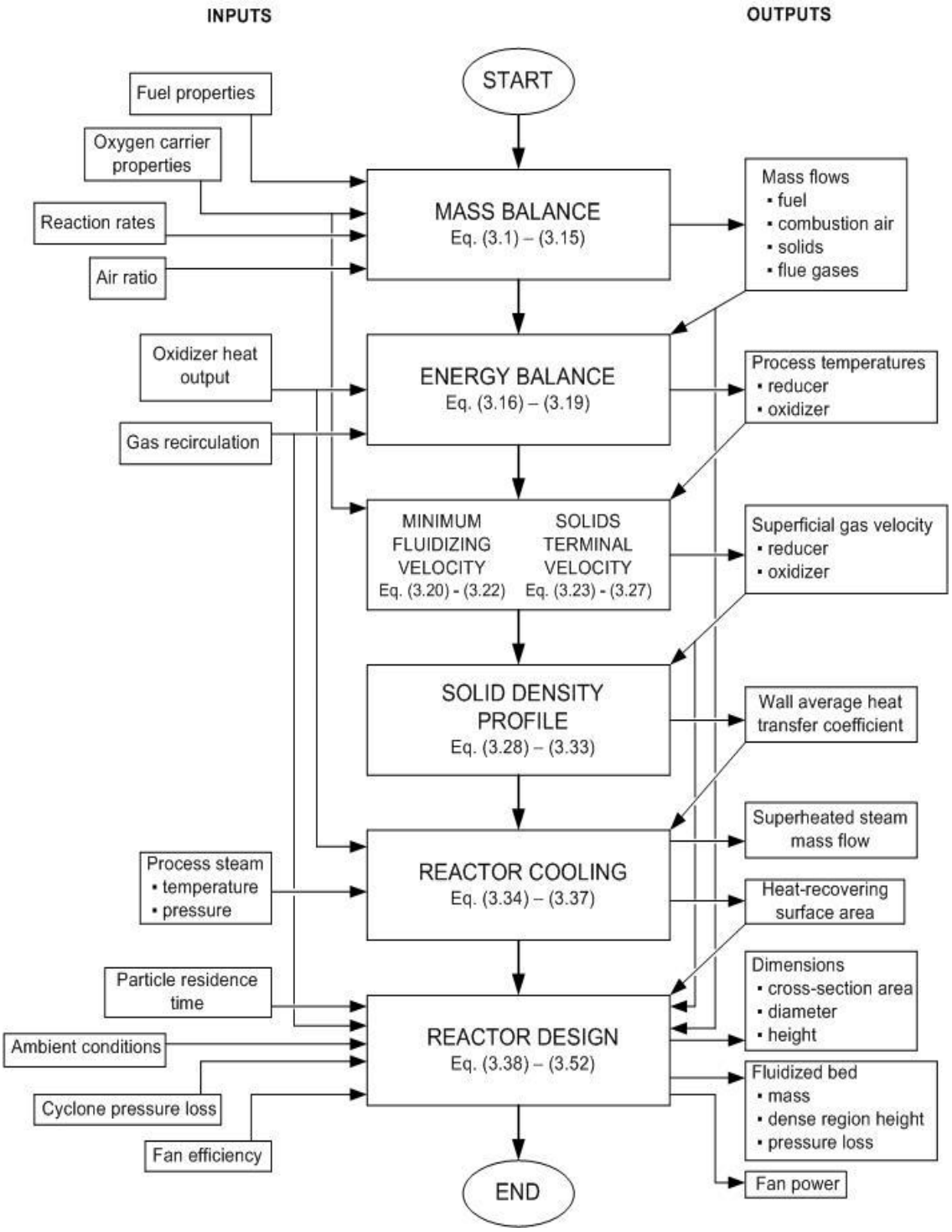

Figure 12. Model structure.

3.2.1 Mass balance equations

A CLC system consists of two interconnected fluidized bed reactors. Mass transfer into the reactors and out of the reactors is governed by the steady state mass balance equations. Mass transfer components and used notations are shown in Figure 13.

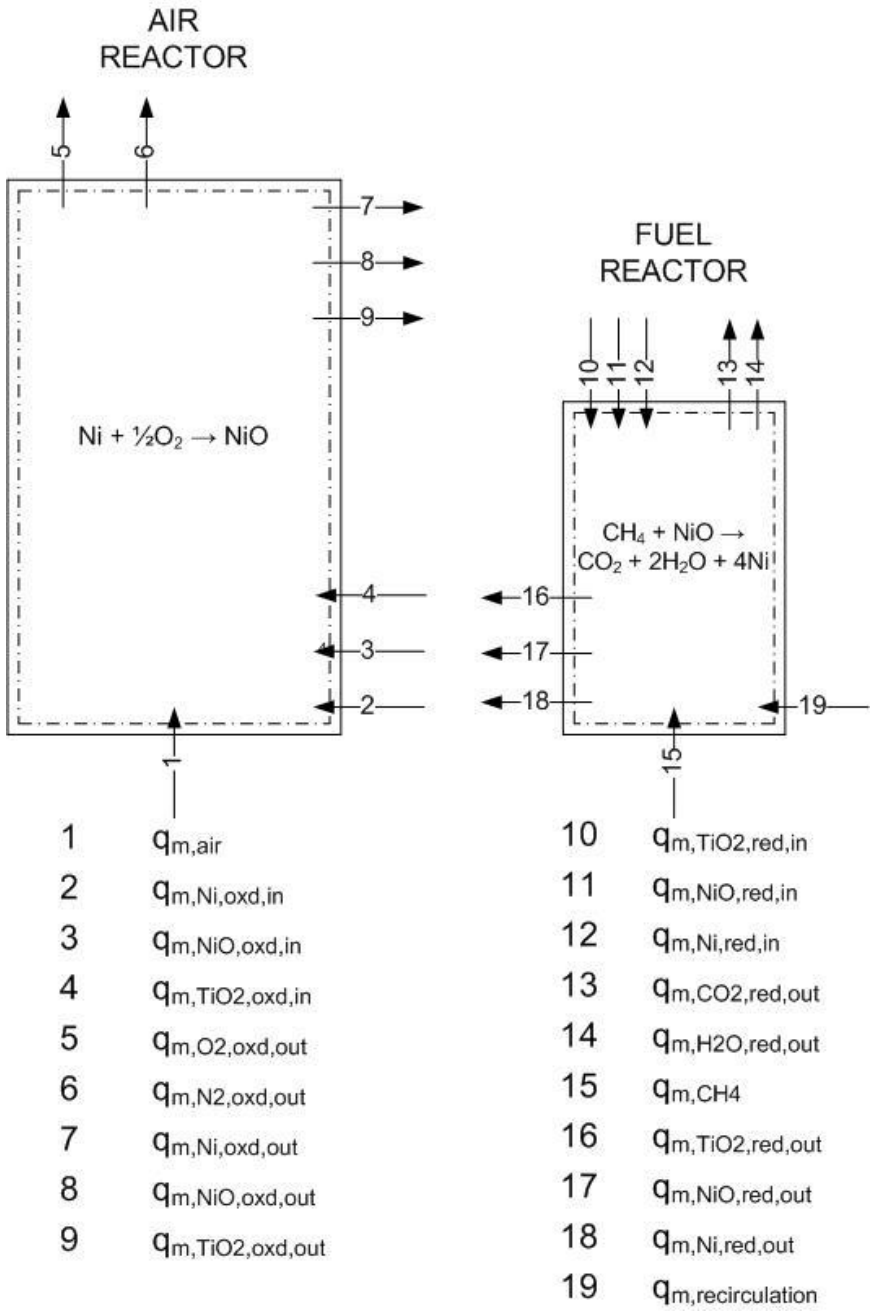

Figure 13. Different mass transfer components of a CLC system.

Presuming that the fuel, i.e. methane, is fully oxidized, the fuel consumption is given by the fuel power, P_{fuel}, and the heating value of methane, $q_{\text{i,CH4}}$:

$$q_{\text{m,CH4}} = \frac{P_{\text{fuel}}}{q_{\text{i,CH4}}} \tag{3.1}$$

The total solids mass flow from the oxidizer to the reducer consists of three components: oxidized and non-oxidized nickel, and inert titanium oxide, as followed

$$q_{\text{m,solid,oxd,out}} = q_{\text{m,NiO,oxd,out}} + q_{\text{m,Ni,oxd,out}} + q_{\text{m,TiO2,oxd,out}} \tag{3.2}$$

$$q_{\text{m,NiO,oxd,out}} = q_{\text{m,NiO,red,in}} = 4q_{\text{m,CH4}} \frac{M_{\text{NiO}}}{M_{\text{CH4}} X_{\text{red}}} \tag{3.3}$$

$$q_{\text{m,Ni,oxd,out}} = q_{\text{m,Ni,red,in}} = q_{\text{m,NiO,oxd,out}} \frac{1 - X_{\text{oxd}}}{X_{\text{oxd}}} \tag{3.4}$$

$$q_{\text{m,TiO2,oxd,out}} = q_{\text{m,TiO2,red,in}} = q_{\text{m,NiO,oxd,out}} \frac{w_{\text{TiO2}}}{w_{\text{NiO}}} + q_{\text{m,Ni,oxd,out}} \frac{w_{\text{TiO2}}}{w_{\text{NiO}}} \frac{M_{\text{NiO}}}{M_{\text{Ni}}} \tag{3.5}$$

where $q_{\text{m,i}}$ is the mass flow of species i

M_{i} is the molar mass of species i

w_{i} is the weight fraction of species i

X is the degree of oxidation/reduction

In the fuel reactor most of the oxygen carrier particles are reduced by the fuel, but some will pass through without reacting. As an inert, the titanium oxide will not react at all during the process. The total mass flow from the reducer to the oxidizer is then

$$q_{\text{m,solid,red,out}} = q_{\text{m,solid,oxd,in}} = q_{\text{m,NiO,red,out}} + q_{\text{m,Ni,red,out}} + q_{\text{m,TiO2,red,out}} \tag{3.6}$$

$$q_{\mathrm{m,NiO,red,out}} = q_{\mathrm{m,NiO,oxd,in}} = q_{\mathrm{m,NiO,red,in}} - 4q_{\mathrm{m,CH4}} \frac{M_{\mathrm{NiO}}}{M_{\mathrm{CH4}}} \tag{3.7}$$

$$q_{\mathrm{m,Ni,red,out}} = q_{\mathrm{m,Ni,oxd,in}} = q_{\mathrm{m,Ni,red,in}} + 4q_{\mathrm{m,CH4}} \frac{M_{\mathrm{NiO}}}{M_{\mathrm{CH4}}} \tag{3.8}$$

$$q_{\mathrm{m,TiO2,red,out}} = q_{\mathrm{m,TiO2,oxd,in}} = q_{\mathrm{m,TiO2,red,in}} \tag{3.9}$$

Flue gas from the reducer contains CO_2 and H_2O:

$$q_{\mathrm{m,CO2,red,out}} = q_{\mathrm{m,CH4}} \frac{M_{\mathrm{CO2}}}{M_{\mathrm{CH4}}} \tag{3.10}$$

$$q_{\mathrm{m,H2O,red,out}} = 2q_{\mathrm{m,CH4}} \frac{M_{\mathrm{H2O}}}{M_{\mathrm{CH4}}} \tag{3.11}$$

The combustion air mass flow is a sum of incoming O_2 and N_2 given by the fuel consumption and the air ratio, λ:

$$q_{\mathrm{m,air}} = q_{\mathrm{m,O2,oxd,in}} + q_{\mathrm{m,N2,oxd,in}} \tag{3.12}$$

$$q_{\mathrm{m,O2,oxd,in}} = 2\lambda q_{\mathrm{m,CH4}} \frac{M_{\mathrm{O2}}}{M_{\mathrm{CH4}}} \tag{3.13}$$

$$q_{\mathrm{m,N2,oxd,in}} = q_{\mathrm{m,N2,oxd,out}} = 7.54\lambda q_{\mathrm{m,CH4}} \frac{M_{\mathrm{N2}}}{M_{\mathrm{CH4}}} \tag{3.14}$$

After the carrier particle oxidation, the remnant O_2 is emitted from the air reactor:

$$q_{\mathrm{m,O2,oxd,out}} = q_{\mathrm{m,O2,oxd,in}} - (q_{\mathrm{m,solid,oxd,out}} - q_{\mathrm{m,solid,oxd,in}}) \tag{3.15}$$

3.2.2 Energy balance equations

The total heat output from the oxidizer and the reducer is denoted by $\Phi = \Phi_{oxd} + \Phi_{red}$. Assuming the temperatures $T_{CO2,red,out} = T_{H2O,red,out} = T_{red}$ and $T_{N2,oxd,out} = T_{O2,oxd,out} = T_{oxd}$, the steady state energy equation for the whole system can be written

$$\begin{aligned} &q_{m,air} c_{p,air}(T_{air})(T_{air} - T_0) + q_{m,CH4}[c_{p,CH4}(T_{CH4})(T_{CH4} - T_0) + q_{i,CH4}] = \\ &q_{m,N2,oxd,out} c_{p,N2}(T_{oxd})(T_{oxd} - T_0) + q_{m,O2,oxd,out} c_{p,O2}(T_{oxd})(T_{oxd} - T_0) + \\ &q_{m,CO2,red,out} c_{p,CO2}(T_{red})(T_{red} - T_0) + q_{m,H2O,red,out} c_{p,H2O}(T_{red})(T_{red} - T_0) + \Phi \end{aligned} \tag{3.16}$$

The additional energy balances may be written separately for the both reactors. If we assume that $T_{NiO,oxd,in} = T_{Ni,oxd,in} = T_{TiO2,oxd,in} = T_{red}$ and $T_{NiO,oxd,out} = T_{Ni,oxd,out} = T_{TiO2,oxd,out} = T_{N2,oxd,out} = T_{O2,oxd,out} = T_{oxd}$, the energy equation for the air reactor is

$$\begin{aligned} &q_{m,air} c_{p,air}(T_{air})(T_{air} - T_0) + q_{m,NiO,oxd,in} c_{p,NiO}(T_{red})(T_{red} - T_0) + \\ &(q_{m,NiO,oxd,in} - q_{m,NiO,oxd,out}) \frac{\Delta H_{c,NiO}}{M_{NiO}} + q_{m,Ni,oxd,in} c_{p,Ni}(T_{red})(T_{red} - T_0) + \\ &q_{m,TiO2,oxd,in} c_{p,TiO2}(T_{red})(T_{red} - T_0) = q_{m,NiO,oxd,out}[c_{p,NiO}(T_{oxd})(T_{oxd} - T_0) + \\ &q_{m,Ni,oxd,out} c_{p,Ni}(T_{oxd})(T_{oxd} - T_0) + q_{m,TiO2,oxd,out} c_{p,TiO2}(T_{oxd})(T_{oxd} - T_0) + \\ &q_{m,O2,oxd,out} c_{p,O2}(T_{oxd})(T_{oxd} - T_0) + q_{m,N2,oxd,out} c_{p,N2}(T_{oxd})(T_{oxd} - T_0) + \Phi_{oxd} \end{aligned} \tag{3.17}$$

The fuel mass flow itself might be too low to maintain adequate fluidization velocity in the fuel reactor. Therefore, the desired amount of combustion gases can be recirculated back into the fuel reactor. Perceiving the gas recirculation, the energy equation for the fuel reactor is

$$\begin{aligned} &q_{m,CH4}[c_{p,CH4}(T_{CH4})(T_{CH4} - T_0) + q_{i,CH4}] + q_{m,NiO,red,in} c_{p,NiO}(T_{oxd})(T_{oxd} - T_0) + \\ &(q_{m,NiO,red,out} - q_{m,NiO,red,in}) \frac{\Delta H_{c,Ni}}{M_{NiO}} + q_{m,Ni,red,in} c_{p,Ni}(T_{oxd})(T_{oxd} - T_0) + \\ &q_{m,TiO2,red,in} c_{p,TiO2}(T_{oxd})(T_{oxd} - T_0) + x_{CO2} q_{m,CO2,red,out} c_{p,CO2}(T_{recirc})(T_{recirc} - T_0) + \\ &x_{H2O} q_{m,H2O,red,out} c_{p,H2O}(T_{recirc})(T_{recirc} - T_0) = q_{m,NiO,red,out} c_{p,NiO}(T_{red})(T_{red} - T_0) + \\ &q_{m,Ni,red,out} c_{p,Ni}(T_{red})(T_{red} - T_0) + q_{m,TiO2,red,out} c_{p,TiO2}(T_{red})(T_{red,out} - T_0) + \\ &(1 + x_{H2O}) q_{m,H2O,red,out} c_{p,H2O}(T_{red})(T_{red} - T_0) + (1 + x_{CO2}) q_{m,CO2,red,out} c_{p,CO2}(T_{red})(T_{red} - T_0) \end{aligned} \tag{3.18}$$

where x_i is the recirculation ratio of gas *i*

T_{recirc} is the temperature of recirculated gas compound

3.2.3. Thermodynamic and physical properties

The specific heat capacity of substance *i* under constant pressure, $c_{\text{p,i}}$, is a function of temperature. Polynomial fit (3.19) with correlation constants of *a*, *b*, *c* and *d* presented in Table 5 was used to calculate specific heat capacities of various gases. (Talonpoika & Sahlberg, 1989).

$$c_{\text{p,i}}(T) = \text{a} + \text{b}T + \text{c}T^2 + \text{d}T^3 \tag{3.19}$$

Table 5. Constants for calculation of the specific heat capacity. (Talonpoika & Sahlberg, 1989).

Gas	*a*	*b*	*c*	*d*	Temperature range (K)
H_2	0.135541	$2.32145 \cdot 10^{-3}$	$-1.49044 \cdot 10^{-6}$	$6.61961 \cdot 10^{-10}$	200 – 1800
N_2	1.03708	$-8.14192 \cdot 10^{-5}$	$3.20231 \cdot 10^{-7}$	$-1.14070 \cdot 10^{-10}$	200 – 1800
O_2	0.829359	$3.33475 \cdot 10^{-4}$	$-6.70968 \cdot 10^{-8}$	$-9.08737 \cdot 10^{-12}$	200 – 1800
H_2O	1.80768	$1.79273 \cdot 10^{-5}$	$6.80617 \cdot 10^{-7}$	$-2.22443 \cdot 10^{-10}$	200 – 1800
CO_2	0.490949	$1.42374 \cdot 10^{-3}$	$-8.71165 \cdot 10^{-7}$	$1.94080 \cdot 10^{-10}$	200 – 1800
CH_4	2.31220	$-3.48737 \cdot 10^{-3}$	$1.31421 \cdot 10^{-5}$	$-7.84784 \cdot 10^{-9}$	200 – 800
Air	0.982076	$1.64395 \cdot 10^{-5}$	$2.25868 \cdot 10^{-7}$	$-8.81495 \cdot 10^{-11}$	200 – 1800

Correlations for calculating the specific heat capacities of solid Ni, NiO and TiO2, are given in Table 6. A thermal anomaly associated with the antiferromagnetic-paramagnetic transformation is observed in the heat capacity of NiO at 519 K by Hemingway (1990). To avoid the complications in the iteration procedure due to discontinuity at specific heat capacity of NiO, a constant specific heat of 718 J/kgK was used at the temperature interval from 410 K to 820 K as shown by solid line in Figure 13.

Table 6. Specific heat capacities of solid materials.

	Temperature range (K)
Ni	
$c_{p,Ni} = 132.91 \cdot \log T - 346.24$	100 – 1500
NiO **	
$a = 4110.72 - 5.302412T + 0.00352061T^2 - 53039.297T^{-0.5} + 2.43067 \cdot 10^7 T^{-2}$	245 – 519
$a = -8.776 + 0.042232T - 7.5267 \cdot 10^{-6} T^{-2} + 787.25T^{-0.5} + 3.6067 \cdot 10^{-6} T^{-2}$	519 – 1800
$c_{p,NiO} = \frac{a}{0.0747}$	
TiO_2	
$c_{p,TiO2} = 230 + 2.6583T - 0.0041T^2 + 3 \cdot 10^{-6} T^3 - 8 \cdot 10^{-10} T^4$	400 – 1200

** Hemingway B. (1990)

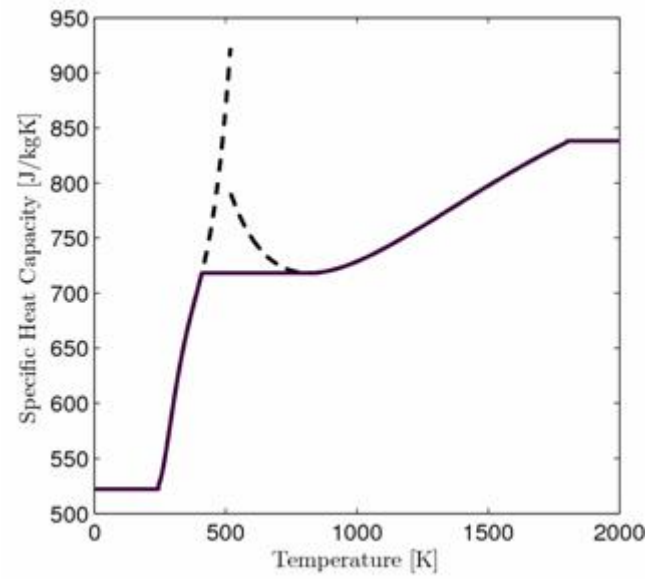

Figure 14. Specific heat capacity of NiO calculated from correlation presented in table 6 (dashed line) and approximation used in the simulations (solid line).

3.2.4 Minimum fluidizing velocity

In a fluidized bed reactor, the onset of fluidization occurs when the drag force of upward moving gas is equal to the weight of the particles. Minimum fluidizing velocity, u_{mf}, can be iterated from the following equation (Kunii & Levenspiel, 1991):

$$\frac{1.75}{\varepsilon_{\mathrm{mf}}^3 \phi_{\mathrm{s}}}\left(\frac{d_{\mathrm{p}} u_{\mathrm{mf}} \rho_{\mathrm{g}}}{\mu}\right)\mathrm{Re}_{\mathrm{p,mf}}^2 + \frac{150(1-\varepsilon_{\mathrm{mf}})}{\varepsilon_{\mathrm{mf}}^3 \phi_{\mathrm{s}}^2}\mathrm{Re}_{\mathrm{p,mf}} = \mathrm{Ar} \tag{3.20}$$

where d_{p} is the particle size

$\varepsilon_{\mathrm{mf}}$ is the voidage at the onset of fluidization

ϕ_{s} is the roundness of particles

μ is the dynamic viscosity of gas

ρ_{g} is the density of gas

The numbers of Archimedes and Reynolds are defined, respectively, as

$$\mathrm{Ar} = \frac{d_{\mathrm{p}}^3 \rho_{\mathrm{g}} (\rho_{\mathrm{s}} - \rho_{\mathrm{g}}) g}{\mu^2} \tag{3.21}$$

$$\mathrm{Re} = \frac{u_{\mathrm{mf}} d_{\mathrm{p}} \rho_{\mathrm{g}}}{\mu} \tag{3.22}$$

where g is the acceleration due to gravity

ρ is the density of solid

3.2.5 Terminal velocity of solids

To maintain solids circulation between the reactors, superficial gas velocity in the air reactor must be higher than terminal falling velocity of solids, u_{T}, which is defined as

$$u_{\mathrm{T}} = \left[\frac{4gd_{\mathrm{p}}}{3C_{\mathrm{D}}} \left(\frac{\rho_{\mathrm{s,oxd}}}{\rho_{\mathrm{air}}} - 1 \right) \right]^{1/2} \tag{3.23}$$

The drag coefficient model by Basu et al. (1991) Eq. (3.24) is a function of the Reynolds number for particles at terminal velocity Eq. (3.25).

$$C_{\mathrm{D}} = \frac{a_1}{\mathrm{Re}_{\mathrm{T}}^{\mathrm{b}}} \tag{3.24}$$

$$Re_{\mathrm{T}} = \frac{u_{\mathrm{T}} d_{\mathrm{p}} \rho_{\mathrm{air}}}{\mu} \tag{3.25}$$

The dynamic viscosity, μ, is calculated as a function of temperature. Eq. (3.26) is valid in a temperature range from $T = 700$ °C to 1250 ºC (Wolf, 2004).

$$\mu = 5.55556 \cdot 10^{-15} T^3 - 2.04475 \cdot 10^{-11} T^2 + 4.79114 \cdot 10^{-8} T + 1.57354 \cdot 10^{-5} \tag{3.26}$$

According to Howard (1989), constants a_1 and b for calculation of the drag coefficient vary in different ranges of the Reynolds number, listed in Table 7

Table 7. Values of a_1 and b with different Reynolds numbers.

Region	Range of Re_{T}	a_1	b
Stoke's law	$0 < Re_{\mathrm{T}} < 0.4$	24	1
Intermediate law	$0.4 < Re_{\mathrm{T}} < 500$	10	0.5
Newton's law	$500 < Re_{\mathrm{T}}$	0.43	0

The terminal falling velocity of NiO/TiO_2 particles (d_{p} = 2.0 mm, ρ = 5195 kg/m^3) used in this study was calculated u_{T} = 2.9 m/s.

3.2.6 Average solids density in the reactor

A fluidization reactor usually has two zones:

i) Bottom bed: a dense bubbling phase having a more or less distinct upper surface separating it from an upper dispersed phase

ii) Freeboard: the section of the reactor between the surface of the dense phase and the exit of the gas stream, in which the density of solid decreases with height.

Experimental findings show, that in the fast fluidization regime carryover of solids is very large and the bottom region is relatively short having a solid fraction of $\varepsilon_B = 0.2 - 0.4$.

When the superficial gas velocity is higher than the terminal falling velocity of solids, a certain amount of particles is projected into the freeboard above the bottom bed. At even higher gas velocities the average density of particles in the freeboard rises. Fig. 14 shows the linear dependence between fluidizing velocity and mean particle density used in this study. At the threshold point, there's no noticeable surface between the bottom bed and freeboard. (Kunii & Levenspiel, 1991).

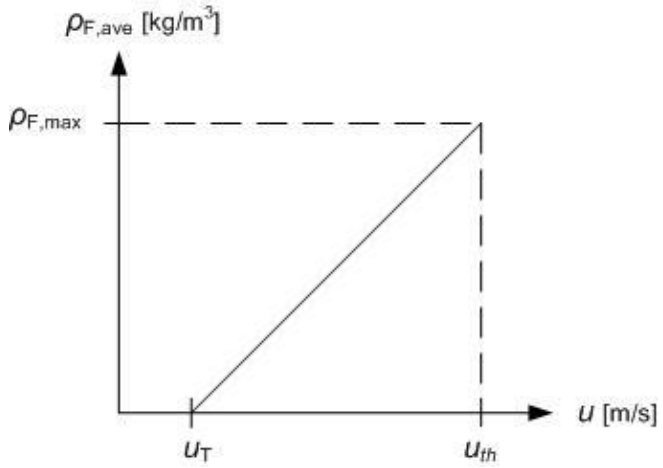

Figure 15. The average density of particles in the freeboard as a function of the fluidizing velocity.

An increase in the superficial gas velocity increases the outgoing solids mass flow from the air reactor until a threshold point is reached. After that, all the solids are blown out of the reactor without any internal recirculation, and an increase in the gas velocity does not affect the solids circulation. The difference in superficial gas velocity and solids terminal velocity can be expressed as

$$\Delta u = u - u_{\mathrm{T}} \tag{3.27}$$

The difference in these two velocities at the threshold point, Δu_{th}, is presumed to be 2.5 m/s, which is quite realistic value for a pneumatic transport reactor according to Naqvi et al. (2007).

The average density of particles in the freeboard, $\overline{\rho}_{\mathrm{F}}$, can be correlated to the superficial gas velocity, u, by the following assumptions:

1 º $\quad \overline{\rho}_{\mathrm{F}} = f(u)$

2 º $\overline{\rho}_{\mathrm{F}}$ increases linearly as a function of u

$$\Rightarrow \quad \overline{\rho}_{\mathrm{F}} = \mathrm{A}u + \mathrm{B}$$

3 º When the superficial gas velocity is lower than or equal to the terminal falling velocity of particles, there is no particle projection into the freeboard.

$$u \le u_{\mathrm{T}}$$

$$\overline{\rho}_{\mathrm{F,T}} = \mathrm{A}u_{\mathrm{T}} + \mathrm{B} = 0 \tag{3.28}$$

$$\Rightarrow \quad \mathrm{A} = -\frac{\mathrm{B}}{u_{\mathrm{T}}} \tag{3.29}$$

4 º When the superficial gas velocity is equal to or higher than the gas velocity at the threshold point, all the solids are blown out of the reactor without any internal recirculation.

$$u \geq u_{\text{th}}$$

$$\bar{\rho}_{\text{F,max}} = \text{A}u_{\text{th}} + \text{B} = -\frac{\text{B}}{u_{\text{T}}}u_{\text{th}} + \text{B} = \text{B}\left(1 - \frac{u_{\text{th}}}{u_{\text{T}}}\right) \tag{3.30}$$

$$\Rightarrow \qquad \text{B} = \frac{\bar{\rho}_{\text{F,max}}}{1 - u_{\text{th}} / u_{\text{T}}} \tag{3.31}$$

5 º Correlation for the average density of particles in the freeboard is valid, when

$$u_{\text{T}} < u < u_{\text{th}}$$

$$\bar{\rho}_{\text{F}} = \text{A}u + \text{B} = -\frac{\text{B}}{u_{\text{T}}}u + \text{B} = \text{B}\left(1 - \frac{u}{u_{\text{T}}}\right) = \left(\frac{\bar{\rho}_{\text{F,max}}}{1 - u_{\text{th}} / u_{\text{T}}}\right)\left(1 - \frac{u}{u_{\text{T}}}\right) \tag{3.32}$$

The maximum density of particles in the freeboard can be expressed as

$$\bar{\rho}_{F,\text{max}} = \varepsilon_{\text{ave}}\rho_{\text{s}} + (1 - \varepsilon_{\text{ave}})\rho_{\text{g}} \tag{3.33}$$

where ε_{ave} is the average solid fraction in the reactor

ρ_s is the density of the solid particles

ρ_g is the density of gas

The average solid density in the freeboard as a function of the superficial gas velocity is shown in Figure 16. The maximum value of $\bar{\rho}_{\text{F}}$ was 21.6 kg/m^3.

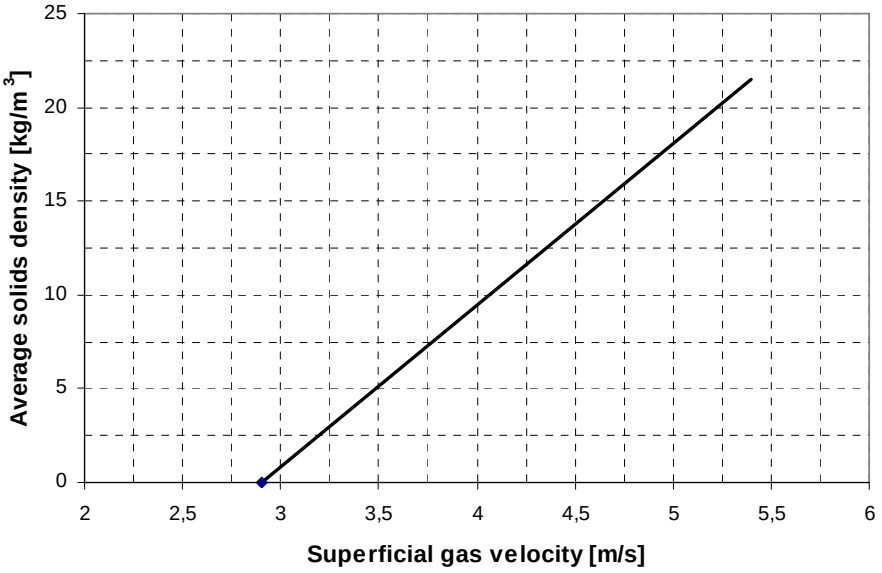

Figure 16. Average solids density in the freeboard as a function of the superficial gas velocity.

3.2.7 Heat transfer

The maximum amount of heat taken from the system is determined by the temperature in the fuel reactor. That temperature must be above the ignition point of the fuel. The reduction reaction is endothermic with most oxygen carriers, which leads to a temperature fall in the fuel reactor. Therefore the fuel reactor is normally not cooled. In this model, the process heat is taken from the air reactor. The cooling of the air reactor can be arranged as in a regular CFB boiler, with heat transfer to the vertical membrane-walls. These walls are exposed to a particle suspension having an almost uniform temperature.

The temperature, T_{sh}, and the pressure, p_{sh}, of superheated steam and the amount of heat, Φ_{oxd}, taken from the air reactor are steam process inputs. The specific enthalpies of saturated water, h', saturated steam, h'', and superheated steam, h_{sh}, can be found from the X Steam Tables for Matlab® by Holmgren (2006).

The mass flow of superheated steam is

$$q_{\mathrm{m,steam}} = \frac{\Phi_{\mathrm{oxd}}}{h_{\mathrm{sh}} - h'} \tag{3.34}$$

The transition from liquid form of water to superheated steam contains two steps:

1) From saturated water to saturated steam

2) From saturated steam to superheated steam.

The required heating power for the first step is

$$\Phi_{\mathrm{sg}} = q_{\mathrm{m,steam}} (h'' - h') \tag{3.35}$$

Similarly for the second step:

$$\Phi_{\mathrm{sh}} = q_{\mathrm{m.steam}} (h_{\mathrm{sh}} - h'') \tag{3.36}$$

Breitzholtz et al. (2001) presented a correlation for the CFB reactor wall average heat transfer coefficient, h_{c} [W/m^{2}K], as a function of the average suspension density in the freeboard, $\overline{\rho}_F$ [kg/m^3]:

$$h_{\mathrm{c}} = h_0 \overline{\rho}_F^{\alpha} \tag{3.37}$$

Such a correlation expresses the total heat transfer, including gas convection, particle convection and radiation. Due to the measurements by Breitzholtz et al. (2001), the dimensionless parameters of Eq. (3.37) were determined to $h_0 = 110$ and $\alpha = 0.21$. Values of h_c are presented in Figure 17.

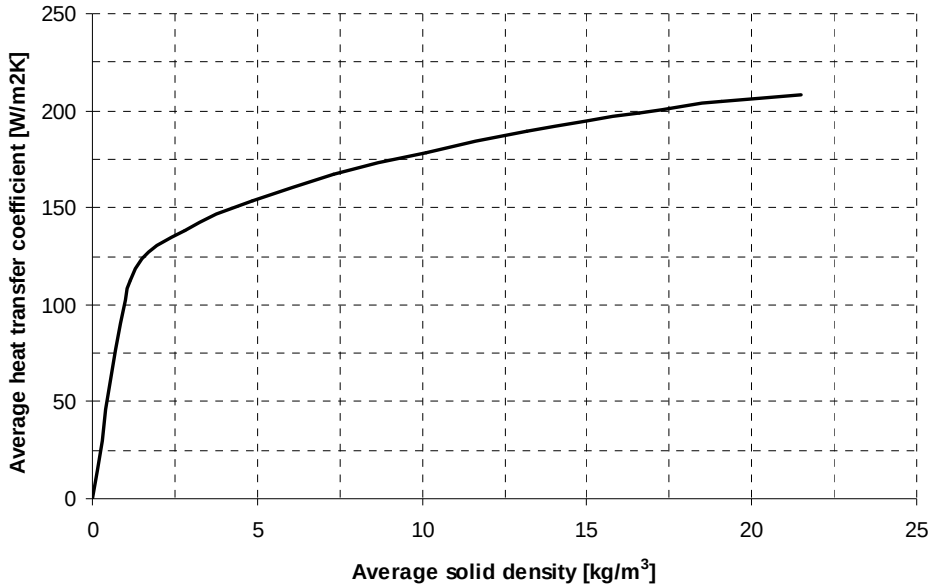

Figure 17. Wall average heat transfer coefficient as a function of the average suspension density in the freeboard.

3.2.8 Air reactor design

The amount of solid bed material in both reactors can be calculated by the following equations:

$$m_{\mathrm{s,oxd}} = q_{\mathrm{m,solid,oxd,in}} \bar{\tau}_{\mathrm{oxd}} \tag{3.38}$$

$$m_{\mathrm{s,red}} = q_{\mathrm{m,solid,\,red,in}} \bar{\tau}_{\mathrm{red}} \tag{3.39}$$

where $\bar{\tau}$ is the mean residence time of oxygen carrier particles in the reactor

Air reactor's cross-sectional area, A, is determined by the volumetric air flow, $q_{\mathrm{V,air}}$, and the fluidization velocity, u_{oxd}:

$$A = \frac{q_{\mathrm{V,air}}}{u_{\mathrm{oxd}}} = \frac{q_{\mathrm{m,air}}}{\rho_{\mathrm{air}} u_{\mathrm{oxd}}} \tag{3.40}$$

The density of air, ρ_{air}, is calculated by using the ideal-gas law:

$$\rho_{\text{air}} = \frac{p_{\text{atm}} M_{\text{air}}}{R T_{\text{oxd}}} \tag{3.41}$$

where p_{atm} is the ambient pressure

M_{air} is the molar mass of air

R is the universal gas constant

The volume of solids in the air reactor is

$$V_{\text{s,oxd}} = \frac{m_{\text{s,oxd}}}{\rho_{\text{s,oxd}}} \tag{3.42}$$

where $\rho_{\text{s,oxd}}$ is the density of oxygen carrier particles

The average solid fraction in the air reactor is

$$\varepsilon_{\text{ave}} = \frac{V_{\text{s,oxd}}}{A H_{\text{oxd}}} \tag{3.43}$$

After determining the maximum density of particles in the freeboard (Eq. 3.33) and the wall heat transfer coefficient (Eq. 3.32), the total area of heat-recovering surfaces, A_{Φ}, may be calculated as follows:

$$A_{\Phi} = \frac{\Phi_{\text{sg}}}{h(T_{\text{oxd}} - T')} \tag{3.44}$$

The air reactor is assumed to have a square-shaped cross-sectional area. Hence, the reactor height will be

$$H_{\text{oxd}} = \frac{A_{\Phi}}{4\sqrt{A}} \tag{3.45}$$

A bottom section that does not contain any heat transfer surfaces is needed due to structural demands of the reactor. Thus, a constant value of 5 meters will be added to the calculated reactor height.

Height of the dense region (bottom bed) in the reactor before any fluidization occurs:

$$H_{\text{B}} = \frac{V_{\text{s}}}{A\varepsilon_{\text{B}}} \tag{3.46}$$

3.2.9 Fuel reactor design

The design of the fuel reactor can be divided into two different approaches. (i) If the recirculation of combustion gases is not applied, low fluidizing velocity is desired due to small volumetric gas flow. In that case, the reducer should be designed as a low-velocity bubbling fluidized bed reactor. (ii) Gas flow in the reducer can be increased by the recirculation of combustion gases. If the combustion gases are recirculated back into the fuel reactor, the fluidizing velocity can be assumed to be somewhat similar to the value in the air reactor. Higher gas velocity increases the solid entrainment rate, and in order to prevent accumulation of solids in the reactor outlet, the superficial gas velocity should be kept in a reasonable level by increasing reactor's diameter or height.

Denoting the gas recirculation ratio (ratio of the total flow of gas supplied into the fuel reactor and the fuel flow) by R_{re}, the reducer cross-section area, A_{red}, is then (Lyngfelt et al., 2001)

$$A_{\text{red}} = \frac{q_{\text{m,CH4}} v_{\text{CH4}} R_{\text{re}}}{u_{\text{red}}} \frac{T_{\text{red}}}{T_{\text{CH4}}} \tag{3.47}$$

where v_{CH4} is the specific volume of incoming fuel

T_{CH4} is the temperature of incoming fuel

u_{red} is the fluidizing velocity

The fluidizing velocity is based on the unconverted fuel. For example, in case of methane as fuel, each fuel molecule is converted to three molecules. Thus, the actual fluidizing velocity increases with a factor of three as the reaction proceeds. (Lyngfelt et al. 2001).

The height of the fuel reactor can be estimated with a method presented by Kunii & Levenspiel (1991, 173).

3.2.10 Pressure drop and fan power

The total pressure drop of the reactor can be calculated by

$$\Delta p_{tot} = \Delta p_b + \Delta p_d + \Delta p_c \tag{3.48}$$

where Δp_b is the pressure drop in fluidized bed

Δp_d is the pressure drop caused by gas distributors

Δp_c is the pressure drop over cyclone

For fast fluidization, roughly 80% of the pressure drop trough the bed is due to the static head according to Kunii & Levenspiel (1991). The pressure drop caused by wall friction is ignored because of the large reactor diameter. Thus, we can write

$$\Delta p_b = 1.2 \frac{m_s g}{A} \tag{3.49}$$

Gas distributors should have a sufficient pressure drop to achieve equal flows over the entire cross section of the bed. Zuiderweg (1967) presented the following rule of

thumb - verified by various analyses - for calculating the required distributor pressure drop:

$$\Delta p_{\mathrm{d}} = 0.4 \Delta p_{\mathrm{b}} \tag{3.50}$$

The pressure drop in cyclones is assumed to be constant.

The fan power, P_{fan}, necessary to overcome the total pressure drop of the reactor is calculated by the flow equation for a reversible adiabatic process and the isentropic efficiency of the fan, η_{fan} (Lyngfelt et al., 2001):

$$P_{\mathrm{fan}} = \frac{n}{n-1} \frac{p_1 v_{\mathrm{a,i}} q_{\mathrm{m,i}}}{\eta_{\mathrm{fan}}} \left[\left[\frac{p_1 + \Delta p_{\mathrm{tot}}}{p_1} \right]^{(n-1)/n} - 1 \right] \tag{3.51}$$

where $q_{\mathrm{m,i}}$ is the mass flow of either air or fuel

$v_{a,i}$ is the specific volume of either air or fuel at ambient conditions

c_{p} is the heat capacity of either air or fuel (assumed to be constant here)

n is the isentropic coefficient

The fractional fan power to overcome the pressure drop, calculated as a function of the fuel power:

$$\varphi_{\mathrm{fan}} = \frac{P_{\mathrm{fan}}}{P_{\mathrm{fuel}}} \tag{3.52}$$

4 RESULTS AND DISCUSSION

The model includes energy and mass balance equations, heat transfer correlations, calculation of averaged solid density in the reactor and a possibility to recirculate combustion gases (H_2O, CO_2) back into the fuel reactor for adequate gas flow. It also includes calculations of reactor geometry, bed pressure loss and required fan power. Various case studies of a CLC system with different process parameters can be done with this model, which will lead to a better understanding of the process and its operation.

4.1 Example case

Process temperatures are mainly determined by conversion and heat transfer rates in both reactors, solids inventory in the system, and air-to-fuel ratio. Using the developed model, the maximum temperature levels were calculated for adiabatic reactors, with 100 % conversion at different excess air ratios. Results for nickel-based oxygen carrier (60 w-% NiO supported by 40 w-% TiO_2) are shown in Figure 15.

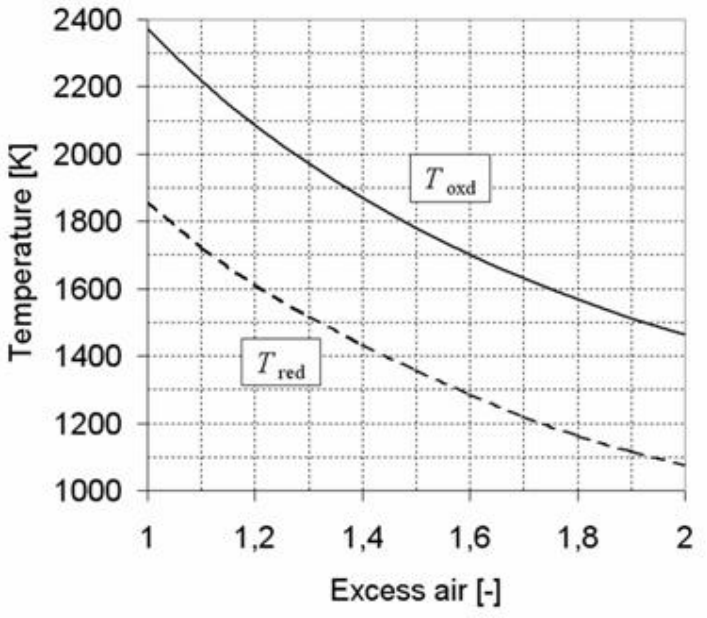

Figure 18. Example case: Adiabatic temperatures of the air reactor, T_{oxd}, and the fuel reactor, T_{red}.

The design parameters and values used in the example case are listed in Table 8. Long enough particle residence times (120 s), based on empirical studies by Adánez et al. (2004), were assumed in the reactors to guarantee conversion rates of 100 %. Excess air ratio of 1.1 was used for the air reactor. Heat is taken from the air reactor by arranging an appropriate cooling. The reduction reaction in the fuel reactor is endothermic, and therefore no additional cooling is required there. Hot flue gases from the reactors contain thermal energy that can be used, for example, to preheat incoming fuel and combustion air. The highest possible operation temperature of a CLC process is determined by the durability of reactor and oxygen carrier materials. Lower limit is given by the minimum temperature required for fuel combustion in the fuel reactor. The reactor temperatures for the studied case are plotted in Figure 16 as a function of air reactor thermal power. Air reactor thermal power Φ_{air} = 57 MW was determined to be used as a design value in the example case, and due to that, the fuel reactor temperature remains just above the auto ignition temperature of methane in air (853 K).

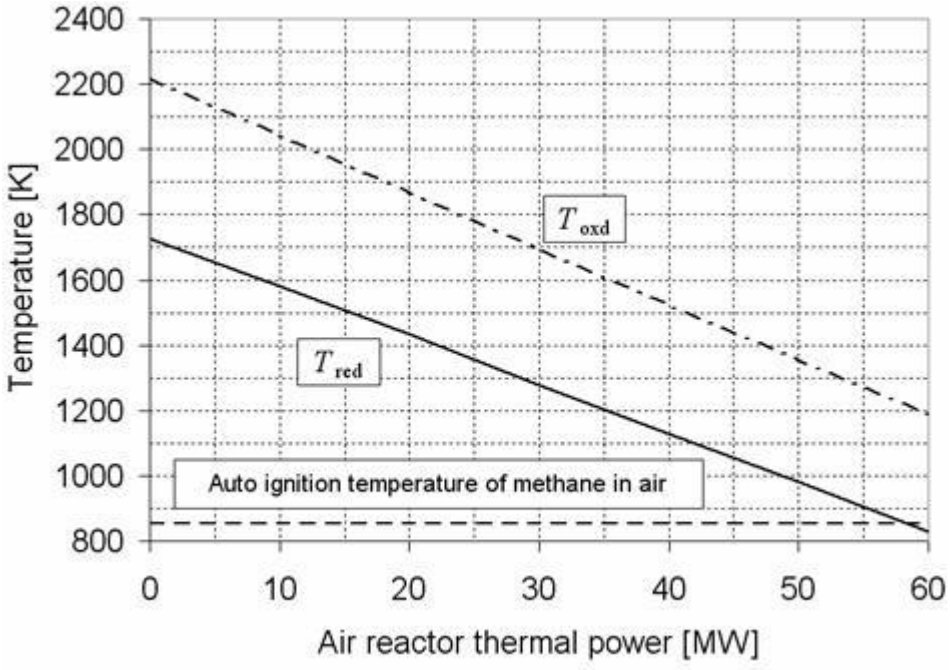

Figure 19. Example case: Temperatures of the air reactor, T_{oxd}, and the fuel reactor, T_{red}, as a function of air reactor thermal power.

Table 8. Example case: chosen or assumed design values.

Item	Symbol	Value	Unit
Fuel power	P_{fuel}	100	MW
Oxidizer heat output	Φ_{oxd}	57	MW
Air ratio	λ	1.1	dimensionless
Degree of oxidation	X_{oxd}	1.0	dimensionless
Degree of reduction	X_{red}	1.0	dimensionless
Mean particle residence time	$\bar{\tau}$	120	s
Gas velocity, oxidizer	u_{oxd}	4.0	m/s
Gas velocity, reducer	u_{red}	1.5	m/s
Fuel temperature	T_{CH4}	300	K
Combustion air temperature	T_{air}	300	K
Superheated steam pressure	p_{sh}	140	bar
Superheated steam temperature	T_{sh}	826	K
Fan efficiency	η_{fan}	0.90	dimensionless
Cyclone pressure drop	Δp_c	1.0	kPa
Bottom bed solid fraction	ε_B	0.35	dimensionless
Oxygen carrier properties (NiO/TiO_2)			
Mass fraction, NiO	w_{NiO}	60	%
Mass fraction, TiO_2	w_{TiO2}	40	%
Density	ρ	5195	kg
Particle size	d_p	0.2	mm

Using design parameters listed in Table 9 together with equations presented in Chapter 3, the temperature levels of the process and mass flow rates of both gaseous and solid substances can be calculated. Results of the example case are shown in Figure 17. Based on the predefined fluidization velocities and required heat transfer areas, rough dimensioning of the air and fuel reactors can be made. First five meters from the bot-

tom of the air reactor was assumed to be masonry and rest of the reactor walls were steam generator membrane tube walls. Fuel reactor was assumed to be uncooled due to the endothermic reaction in the reactor. A schematic picture of reactor dimensions as well as required fan power calculated from the reactor pressure drop is shown in Figure 18.

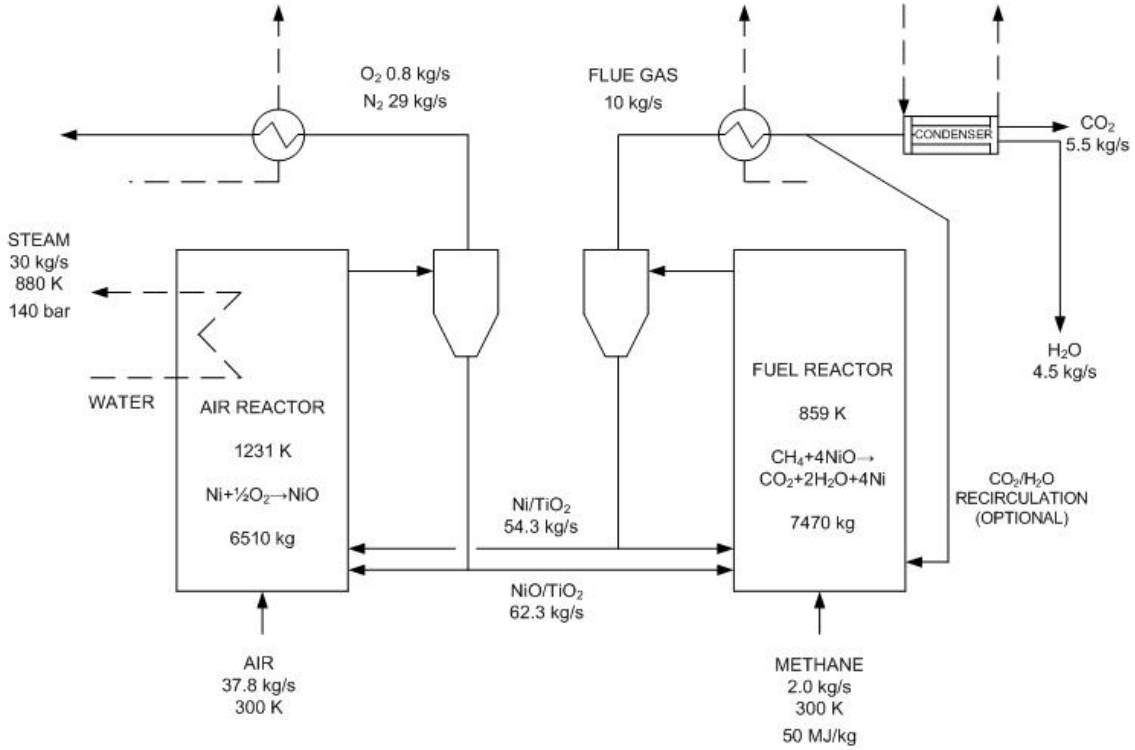

Figure 20. Example case: Temperature levels and mass flow rates given by the steady state mass and energy balance equations.

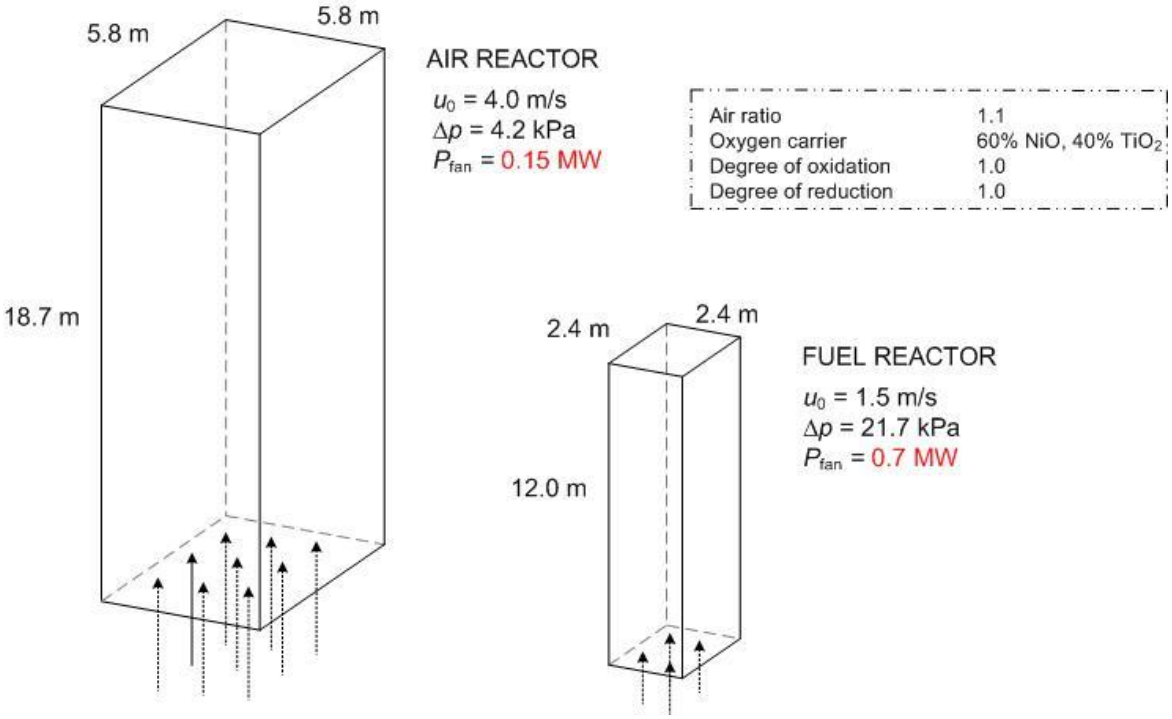

Figure 21. Example case: Reactor dimensions and required fan power.

The relation between reaction rates and solids inventory in the system was also investigated. It became evident, as expected, that in order to reduce costs by minimizing the amount of oxygen carrier material in the reactors, the degrees of both, oxidation and reduction, should be as high as possible, which can be seen in Figure 19. On the other hand, greater amount of bed material in the reactor makes heat transfer more effective. These aspects should be considered when deciding the oxygen carrier type and its optimal amount in the system.

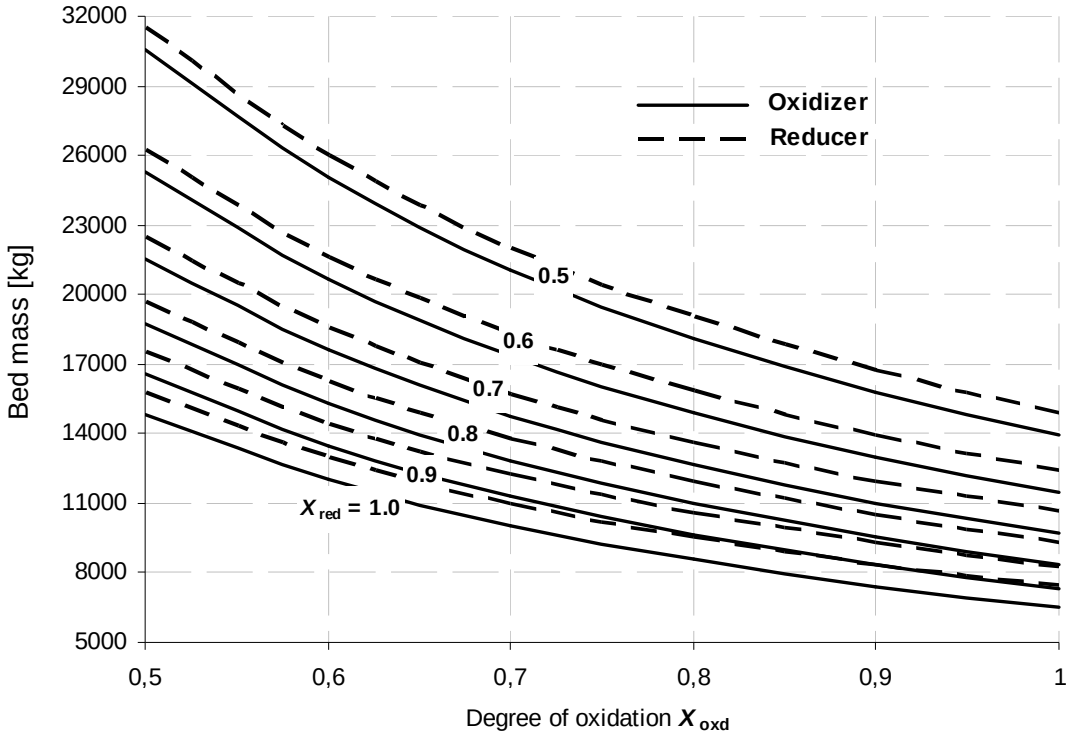

Figure 22. Example case: Bed mass in the reactor as a function of the degree of oxidation/reduction. Air to fuel ratio is 1.1.

4.2 Further development of the model

The developed zero-dimensional model gives an overall view and understanding of the CLC process. The next step is an one-dimensional, time dependent (or steady state) model, which will describe the behavior of the process and combustion dynamics more accurately. In the dynamical one-dimensional model, the reactor is divided into several control volumes. Mass balances for main gas components and volatile compounds are calculated for each control volume against the time. Heat transfer between flue gas, particles and walls in every control volume will also be calculated. In the 0-D model, the temperature inside the reactor is constant. 1-D model accommodates the solid mixing between the control volumes, and therefore the temperature field may vary. Also, the solid density profile over the furnace will be more realistic due to the use of empirical correlations.

5 CONCLUSIONS

For this thesis, chemical-looping combustion was studied first based on the literature and then based on the developed steady state process model. CLC can be considered as a promising combustion technique with low energy penalty from the carbon capture. Several studies related to CLC process performance have proposed relatively high net thermal efficiencies in comparison to processes with conventional combustion methods.

At the moment there exist no large scale CLC facilities, but some data from the existing CLC prototype units and conventional larger scale CFB boilers was used in the process modeling. However, very accurate generalizations of the process dynamics cannot be made yet, because the fluid dynamic properties of the oxygen carrier particles used in a CLC system differ quite a lot from those used in a regular CFB boiler, and thus the use of a correlation intended for CFBs may not be justified. The model, however, describes the physics of the process rather realistically and it can be improved when more experimental data is available. Various case studies of a CLC system with different process parameters can be done with the model, which helps to determine the limits and operation range of the CLC process.

Successful commercialization of power generation processes with the integration of CLC depends on the development of both specific process configurations and suitable reactor design**.** There are still many challenges related to oxygen carrier materials, large scale effects and process stability in long-term use.

REFERENCES

Adánez, J., de Diego, L. F., García-Labiano, F., Gayán, P., Abad, A. (2004). Selection of oxygen carriers for chemical-looping combustion. Energy & Fuels, 18: 371 – 377.

Adánez, J., Abad, A., García-Labiano, F., de Diego, L. F., Gaýan, P., Celaya, J. (2006). Mapping of the range of operational conditions for Cu-, Fe-, and Ni-based oxygen carriers in chemical-looping combustion. Chemical Engineering Science, 62: 533 – 549.

Basu, P. & Fraser, S. (1991). Circulating fluidised bed boilers – Design and operations. Butterworth-Heinemann. Boston, USA. ISBN 0-7506-9226-X.

Berquerand, N. & Lyngfelt, A. (2008). Design and operation of a 10 kWth chemical-looping combustor for solid fuels – Testing with South African coal. Fuel, 87: 2713 – 2276.

Breitzholtz, C., Leckner, B., Baskakov, A. P. (2001). Wall average heat transfer in CFB boilers. Powder Technology, 120: 41 – 48.

García-Labino, de Diego, L. F., Adánez, J., Abad, A., Gaýan P. (2004). Temperature variations in the oxygen carrier particles during their reduction and oxidation in a chemical-looping combustion system. Chemical Engineering Science, 60: 851 – 862.

Hemingway, B. (1990). Thermodynamic properties for bunsenite, NiO, magnetite, Fe3O4, and hematite, Fe2O3, with comments on selected oxygen buffer reactions. American Mineralogist, 75: 781 – 790.

Holmgren, M. (2006). X steam for Matlab. Internet: www.x-eng.com.

Hossain, M. & de Lasa, H. (2008). Chemical-looping combustion (CLC) for inherent CO2 separation – A review. Chemical Engineering Science, 18: 4433 – 4451.

Howard, J.R. (1989). Fluidised bed technology - Principles and application. Adam Hilger. Bristol, United Kingdom. ISBN 978-0852740552.

IEA. (2003). CO2 emissions from fuel combustion 1971/2001 – 2003 edition. ISBN 9264102256.

IPCC. (2001). Climate change 2001: synthesis report. A contribution of working groups I, II, and III to the third assessment report of the Integovernmental Panel on Climate Change [Watson, R.T. and the Core Writing Team (eds.)]. Cambridge University Press, Cambridge, United Kingdom, and New York, NY, USA.

Ishida, M., Zheng, D., Akehata, T. (1987). Evaluation of a chemical-looping combustion power-generation system by graphic exergy analysis. Energy, 2: 147 – 154.

Jerndal, E., Mattisson, T., Lyngfelt, A. (2006). Thermal analysis of chemical-looping combustion. Chemical Engineering Reasearch and Design, 84: 795 – 806.

Johansson, E., Mattisson, T., Lyngfelt, A., Thunman, H. (2006). A 300 W laboratory reactor system for chemical-looping combustion with particle circulation. Fuel, 85: 1428 – 1438.

Johansson, M. (2007). Screening of oxygen-carrier particles based on iron-, manganese-,copper- and nickel oxides for use in chemical-looping technologies. Chalmers University of Technology, Göteborg, Sweden. ISBN 978-91-7385-037-7.

Kronberger, B., Lyngfelt, A., Löffler, G., Hoffbauer H. (2005). Design and fluid dynamic analysis of a bench-scale combustion system with CO2 separation – Chemical-looping combustion. Industrial & Engineering Chemistry Research, 44: 546 – 556.

Kunii, D. & Levenspiel, O. (1991). Fluidization engineering, 2nd edition. Butterworth-Heinemann. USA. ISBN 0-409-90233-0.

Leion, H., Mattisson, T., Lyngfelt, A. (2008). Solid fuels in chemical-looping combustion. International Journal of Greenhouse Gas Control, 2: 180 – 193.

Lyngfelt, A., Leckner, B., Mattisson, T. (2001). A fluidized-bed combustion process with inherent CO2 separaration; application of chemical-looping combustion. Chemical Engineering Science, 56: 3101 – 3113.

Mattisson, T., Johansson, M., Lyngfelt, A. (2006a). CO2 capture from coal combustion using chemical-looping combustion – Reactivity investigation of Fe, Ni and Mn based oxygen carriers using syngas. Proceedings of the Clearwater Coal Conference, Clearwater, Florida, USA, 2006.

Mattisson, T., Zafar, Q., Johansson, M., Lyngfelt, A. (2006b). Chemical-looping combustion as a new CO2 management technology. Proceedings of the First Regional Symposium on Carbon Management, Dhahran, Saudi-Arabia, May 22 – 24, 2006.

Naqvi, A. Wolf, J., Bolland, O. (2007). Part load analysis of a chemical looping combustion (CLC) combined cycle with CO2 capture. Elsevier Energy, 32: 360 – 370.

Richter, H. & Knoche, K. (1983). Reversibility of combustion processes. ACS Symposium Series, 235: 71 – 86.

Rydén, M. (2008). Hydrogen production by reforming of natural gas with carbon dioxide capture by chemical-looping combustion. Chalmers University of Technology, Göteborg, Sweden. ISBN 978-91-7385-108-4.

Rydén, M. & Lyngfelt, A. (2006). Using steam reforming to produce hydrogen with carbon dioxide capture by chemical-looping combustion. International Journal of Hydrogen Energy, 31: 1271 – 1283.

Ryu, H., Jin, G., Yi, C. (2004). Demonstration of inherent CO2 separation and no NOx emission in a 50kW chemical-looping combustor: continuous reduction and oxidation

experiment. Proceedings of the 7th International Conference on Greenhouse Gas Control Technologies, Vancouver, Canada.

Talonpoika, T. & Sahlberg, P. (1989). Thermodynamics course handout. Lappeenranta University of Technology. Lappeenranta, Finland.

Wolf, J. et al. (2001). Performance analysis of combined cycles with chemical looping combustion for CO2 capture. Proceedings of the 18th Annual International Pittsburgh Coal Conference, Newcastle, New South Wales, Australia, pp. 1122 – 1139.

Wolf, J. (2004). CO2 mitigation in advanced power cycles – Chemical looping combustion and steam-based gasification. KTH - Royal Institute of Technology. Universitetsservice US AB, Stockholm, Sweden. ISBN 91-7283-913-9.

Zuiderweg, F. J. (1967). Proceedings of international symposium on fluidization, A.A.H. Drinkenburg, ed., p. 739, Netherlands Univ. Press, Amsterdam.